Available online at www.sciencedirect.com
ScienceDirect
Icarus 196 (2008) 459–476
ICARUS
www.elsevier.com/locate/icarus

Experimental study of the sublimation of ice through an unconsolidated clay layer: Implications for the stability of ice on Mars and the possible diurnal variations in atmospheric water

Vincent Chevrier [a,*], Daniel R. Ostrowski [a], Derek W.G. Sears [a,b]

[a] *W.M. Keck Laboratory for Space Simulation, Arkansas Center for Space and Planetary Sciences, University of Arkansas, Fayetteville, AR 72701, USA*
[b] *Department of Chemistry and Biochemistry, University of Arkansas, Fayetteville, AR 72701, USA*

Received 20 April 2007; revised 28 February 2008

Available online 28 March 2008

Abstract

We have studied the sublimation of ice and water vapor transport through various thicknesses of clay (<63 μm grain size). We experimentally demonstrate that both adsorption and diffusion strongly affect the transport of water, and that the processes of diffusion and adsorption can be separately quantified once the system comes to a steady state. At shallow depths of clay, water vapor transport is determined by diffusion through both the atmosphere and the clay layer, whereas at greater depth the rate of sublimation of the ice is governed only by diffusion through the clay. Using two different models, we determine the diffusion coefficient for water vapor through unconsolidated clay layer to be $1.08 \pm 0.04 \times 10^{-4}$ and $1.29 \pm 0.06 \times 10^{-4}$ $m^2\,s^{-1}$. We also determined the adsorption isotherms for the clay layer, which follow the Langmuir theory at low water vapor pressure (<100 Pa, where a monolayer of water molecules forms on the surface of the clay) and the BET theory at higher pressure (where multiple water layers form). From our analysis of both types of isotherms we determined the adsorption constants to be $\alpha = 4.9 \pm 1.0 \times 10^{-2}$ Pa^{-1} and $c = 30 \pm 10$, respectively, and specific surface areas of $1.10 \pm 0.2 \times 10^5$ and $9.0 \pm 0.7 \times 10^4$ $m^2\,kg^{-1}$, respectively. Finally, we report a theoretical kinetic model for the simultaneous diffusion and adsorption from which we determine adsorption kinetic constants according to the Langmuir theory of $k_a = 2.5 \pm 0.5 \times 10^{-4}$ s^{-1} and $k_d = 8.7 \pm 3.6 \times 10^{-5}$ s^{-1}. If the martian regolith possesses diffusive properties similar to those of the unconsolidated montmorillonite soil we investigated here, it would not represent a significant barrier to the sublimation of subsurface ice. However, at the low subsurface temperatures of high latitude (180 K on average), ice could survive from the last glaciation period (about 300 to 400,000 years ago). Higher subsurface temperatures in the equatorial regions would prevent long-timescale survival of ice in the shallow subsurface. In agreement with previous work, we show that adsorption of water by a clay regolith could provide a significant reservoir of subsurface water and it might account for the purported diurnal cycle in the water content of the atmosphere.

Keywords: Mars, surface; Regolith; Ice; Clays

1. Introduction

Water ice has mostly been observed on the surface of Mars in the polar caps (Bibring et al., 2004) and in the subsurface layers by the gamma ray spectrometer (GRS) and the neutron spectrometers on Mars Odyssey (Boynton et al., 2002; Feldman et al., 2004b). The stability of ice on Mars depends mostly on the thermal properties of the regolith, and factors that determine favorable temperature such as latitude and depth. The depth of the stable ice table increases with decreasing latitude (Clifford and Hillel, 1983; Farmer and Doms, 1979; Leighton and Murray, 1966; Mellon and Jakosky, 1993; Paige, 1992; Schorghofer and Aharonson, 2005; Schorghofer, 2007). All these models show that ice is unstable in equatorial regions at geologically short timescales. Therefore, concentrations of water in the equatorial regions can be attributable to water-rich minerals such as magnesium sulfates (Feldman et al., 2004a; Jakosky et al., 2005) and metastable water ice (Chevrier et al., 2007; Bandfield, 2007). Recent observations performed by

* Corresponding author. Fax: +1 479 575 7778.
E-mail addresses: vchevrie@uark.edu (V. Chevrier), dostrow@uark.edu (D.R. Ostrowski), dsears@uark.edu (D.W.G. Sears).

0019-1035/$ – see front matter
doi:10.1016/j.icarus.2008.03.009

Mars Express OMEGA have also shown abundant clay deposits on the southern Noachian crust of Mars (Poulet et al., 2005). Clays have a strong adsorption capacity due to their large specific surface area and the affinity of the water molecule for the clay crystalline structure, and this makes them potential reservoirs of water on the surface of Mars (Mooney et al., 1952; Anderson et al., 1967, 1978).

Variations in obliquity of Mars have resulted in large-scale transfer of water vapor from the equator to the poles, so subsurface equatorial water deposits might be explained as relics of high obliquity periods (Head et al., 2003; Schorghofer, 2007). Suggestions of Amazonian glacial activity in the equatorial regions are consistent with this hypothesis (Head et al., 2006a, 2006b; Milkovich et al., 2006; Neukum et al., 2004). These observations and models suggest that metastable subsurface ice at medium latitudes could explain the Mars Odyssey observations.

The distribution of ice on Mars is governed by both equilibrium thermodynamics and kinetics. Therefore, laboratory studies of both non-equilibrium and equilibrium processes are of value in attempting to fully characterize the distribution and dynamics of water on Mars. The kinetics of water transfer from the subsurface to the martian atmosphere are largely dependent on the regolith diffusion and adsorption properties, which can be studied through experiments on analogues such as basalt (Fanale and Cannon, 1971; Bryson et al., 2008) or palagonitic soil JSC Mars-1 (Chevrier et al., 2007). This paper describes experiments on the sublimation of subsurface ice below a clay regolith and the development of a numerical transport model of water vapor in porous adsorbent regolith, including simultaneous diffusion and adsorption.

2. Methods

The clay studied in this experiment is a montmorillonite from Panther Creek, Colorado (Ward's Natural Science #46E0438). Since grain size is an important parameter in our experiments, the montmorillonite was sieved to less than 63 μm, which corresponds to the standard grain size for silt sediments. We used a #230 US Standard Testing Sieve with a 63 μm nominal opening and a Humboldt MFG. Co shaker. The shaker was set for 30 min and then the <63 μm montmorillonite was emptied. The shaking process was repeated for another 30 min.

The montmorillonite samples were dried by baking in a Precision Scientific Company, model #1404 vacuum oven at $102 \pm 1\,^{\circ}C$ and 35 mbar for one day. After baking, the samples were transferred to a desiccator and stored in a freezer at $-20\,^{\circ}C$ for one day to maintain dryness and to ensure that the clay did not melt the ice when they came into contact.

Columns of ice covered with regolith were prepared from distilled water frozen in 125–500 mL 5.9–6.4 cm diameter Nalgene cups. The cylinders of ice were sanded to a flat surface with a height that would allow the required clay depth to reach rim of the cup. A thermocouple was then frozen onto the surface of the ice and 2 to 75 mm deep layers of cold and dry clay were placed on the ice (Fig. 1).

We used the simulation chamber and similar set-up procedures to those described in previous publications (Chevrier et al., 2007; Sears and Chittenden, 2005; Sears and Moore, 2005). The 0.6 m^3 chamber was evacuated to less than 0.09 mbar and then filled with dry CO_2 gas to atmospheric pressure. The chamber was then cooled below 0 °C by flowing a methanol/dry ice slurry through cooling coils. Once cooled, the chamber was opened and the sample placed on a Sartorius GE812 top-loading balance (precision of 0.01 g). Then the platform was lowered into the chamber and the lid sealed (Fig. 1). The chamber was evacuated to 7 mbar. The temperature of the chamber was maintained at or below 0 °C to prevent melting of the ice. Experiments varied from 2 h (appropriate for 0.2 cm thickness of clay) to 7 h (appropriate for 7.5 cm thickness of clay). To prevent accumulation of water vapor during the experiment, CO_2 was continuously injected in the atmosphere and the pump was run to maintain a constant pressure of 7 mbar. Using LabView 7.1 software, the mass, pressure, temperature, and humidity were recorded every minute for each experiment. Operating the balance under the extreme conditions in the chamber caused the balance to drift a reproducible 0.10–0.11 g during the first 14 min of the experiments. Our data have been corrected for this effect. At the end of each experiment the water absorbed by the clay was determined by heating in the same vacuum oven at $102 \pm 1\,^{\circ}C$ and 35 mbar and measuring the mass difference.

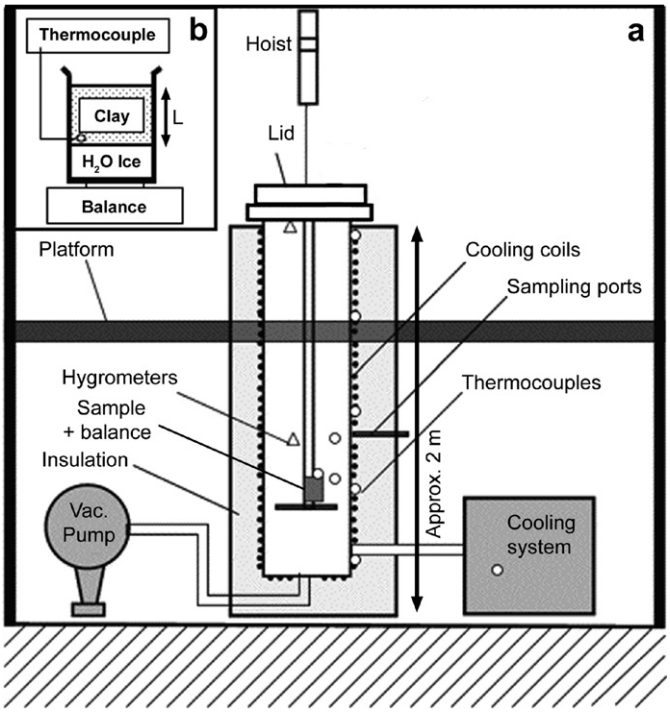

Fig. 1. Schematic diagram of the experimental setup, adapted from Chevrier et al. (2007). (a) The 0.6 m^3 simulation chamber with the positions of the thermocouples (circles) and hygrometers (triangles) indicated. (b) Schematic diagram for the sample set-up, which consists of a pure water ice layer covered with a layer of clay with a depth L and with a thermocouple at the interface. This is set on platform in the chamber a top loading balance.

3. Results

All symbols, constants and variables used in this study are summarized in Table 1. Our results are shown in Table 2. We

Table 1
Summary of mathematical symbols used in this study

A_S	Regolith specific surface area ($m^2\,kg^{-1}$)	R	Ideal gas constant ($8.314\,J\,mol^{-1}\,K^{-1}$)
B	Constant in Eq. (6), defined in Eq. (7)	R_a	Adsorption rate ($m^2\,m^{-2}\,kg^{-1}\,s^{-1}$)
c	Adsorption constant in BET theory	R_d	Desorption rate ($m^2\,m^{-2}\,kg^{-1}\,s^{-1}$)
C_a	Adsorbed concentration ($mol\,m^{-3}$)	T	Temperature (K)
C_g	Pore gas concentration ($mol\,m^{-3}$)	t_1	Time of initial CO_2/H_2O desorption observed in the data (s)
D	Diffusion coefficient ($m^2\,s^{-1}$)	t_2	Time to reach steady-state in the data (s)
D'	Diffusion coefficient including adsorption effect ($m^2\,s^{-1}$)	T_{atm}	Atmospheric temperature (K)
E_0	Sublimation rate of free water ice ($m\,s^{-1}$)	T_S	Surface temperature (K)
E_1	Enthalpy of adsorption of the first molecule layer ($J\,mol^{-1}$)	t_{SS}	Time to reach steady-state in diffusion process (s)
E_C	Enthalpy of condensation ($J\,mol^{-1}$)	v	Volume of adsorbed gas in BET theory ($m^3\,kg^{-1}$)
E_S	Sublimation rate of water ice below a layer of regolith ($m^2\,s^{-1}$)	v_m	Volume of one monolayer of adsorbed gas ($m^3\,kg^{-1}$)
h	Scale height of the atmosphere (m)	z	Depth (m)
J	Flux of molecules ($kg\,m^{-2}\,s^{-1}$)	α	Adsorption constant in Langmuir theory (Pa^{-1})
k_a	Adsorption kinetic constant (s^{-1})	δ	Thickness of ice layer in the martian subsurface (m)
k_d	Desorption kinetic constant (s^{-1})	ε	Thickness of adsorbent regolith on Mars (m)
L	Thickness of regolith layer (m)	θ	Relative surface coverage of adsorbed molecules ($m^2\,m^{-2}\,kg^{-1}$)
l	Thickness of adsorbed molecular layer (m)	ρ_{H_2O}	Density of liquid water ($kg\,m^{-3}$)
m_a	Relative mass of adsorbed molecules ($kg\,kg^{-1}$)	ρ_{ice}	Density of water ice ($kg\,m^{-3}$)
M_{H_2O}	Molecular mass of water ($kg\,mol^{-1}$)	ρ_{reg}	Density of regolith ($kg\,m^{-3}$)
p	Atmospheric water vapor (Pa)	ξ	Amount of water in the martian atmosphere (pr μm)
p_{sat}	Saturation water vapor pressure (Pa)	Ψ	Thermodynamic constant in Eq. (21), defined in Eq. (22)
P	Total gas pressure (Pa)		

will describe the results in terms of mass loss throughout the experiment, time to reach steady state, and the temperature dependence of the sublimation process.

3.1. Mass loss curves

We refer to our plots of the mass of the ice-clay assemblage versus time as mass-loss curves. These mass-loss curves show a variety of shapes depending on the time and thickness of regolith (Fig. 2). Fig. 2a shows the mass loss curves typical of the shallowest depths, where the curves are nearly linear with only a slight decrease in the rate of loss that results mostly from a rapid build up of humidity (Fig. 3). Fig. 2b shows the mass-loss curves for samples with clay layers in excess of 5 mm in which there is a slight increase in slope (at 10 min in the example) followed by a decrease, after about 70 min in this example. Figs. 2c–2f show mass loss curves for depths greater than 30 mm in which a steep initial slope is followed by an almost flat period that increases in duration with increasing regolith depth. To our knowledge it is the first time that such flat phase (which we will refer to as the "transition zone") has been observed in such experiments. Previously, mass-loss curves were monotonic throughout the experiment (Bryson et al., 2008; Chevrier et al., 2007; Hudson et al., 2007).

The rapid loss of mass during the first 20–30 min of our experiments, especially with greater depths of clay, is almost certainly due to the release of carbon dioxide absorbed on the clay grains during set-up in the chamber (we decrease the atmospheric pressure from 1 atm to 7 mbar of CO_2). Zent and Quinn (1995) commented on the ability of clay to adsorb CO_2 and the 20 min or so during set-up when the clay was in 1 atm of pure CO_2 would provide an unavoidable opportunity for this. In the same time, the martian regolith is probably largely in equilibrium with the CO_2 atmosphere, thus our experiments appear to be closer to the reality than if using only water. The transition zone is almost certainly due to water vapor subliming from the ice being absorbed on to the clay with no net loss of water from the system.

3.2. Steady state conditions and dependence of sublimation rate on clay layer thickness

The third and longest period of our experiments is when our sample mass shows a linear decrease with time. Regression coefficients (R^2) for this part of the mass-loss curve were better than 0.95. During this period we have steady state conditions when water vapor sublimed from the ice is at equilibrium with the clay and passes through the column. This, of course, is the period of most interest to us. As expected, and apparent from Fig. 2 (allowing for changes in the time axis), the slopes of the mass-loss curves during steady state decrease with increasing clay layer thickness (Bryson et al., 2008; Chevrier et al., 2007; Hudson et al., 2007).

We determined the time to reach the beginning of the transition zone, t_1, and the beginning steady state conditions, t_2, by subtracting the regression line from the experimental data. We obtain plots like that shown in Fig. 4. We consider deviations significant when they exceed 10%. Values of t_1 and t_2 are included in Table 2. Of most significance to the present work is the time to reach steady state t_2, which increases with increasing clay layer thickness according to a power law (Fig. 5).

The abundance of adsorbed water in our clay layers, measured after the system had achieved steady state, showed a strong depth-dependence (Fig. 6), being highest at shallow depths because of lower temperatures and higher humidity. Adsorption will be discussed in Section 4.2.

Table 2
Measured data during the sublimation experiments of ice below montmorillonite clay regolith

Duration (min)	Av. T_S[b] (K)	$T_{S\ (end)}$[c] (K)	T_{atm} (K)	$RH_{(t=0)}$ (%)	$RH_{(end)}$ (%)	t_1[d] (min)	t_2[d] (min)	E_S[e,f] (mm h^{-1})	Corr. E_S[g] (mm h^{-1})	Water content (wt%)
L[a] = 2 mm										
141	262.9	263.6	273.1	5.4	34.3	n.d.	n.d.	0.921	1.321	8.11
141	265.2	265.4	273.1	5.0	31.4	n.d.	n.d.	0.483	0.729	6.24
141	265.9	269.0	273.1	4.2	33.7	n.d.	n.d.	0.464	0.729	7.26
142	263.6	264.8	273.1	4.1	34.5	n.d.	n.d.	0.807	1.180	7.75
141	264.3	265.5	273.1	3.5	32.5	n.d.	n.d.	0.599	0.882	7.03
L = 5 mm										
141	268.2	267.2	272.7	2.8	30.3	n.d.	n.d.	0.229	0.390	5.04
125	264.8	265.1	272.8	4.5	23.9	n.d.	n.d.	0.455	0.660	5.27
125	264.6	265.1	272.9	4.4	28.5	n.d.	n.d.	0.485	0.710	5.53
L = 10 mm										
137	266.9	267.1	272.5	2.3	24.4	n.d.	4	0.207	0.316	4.31
141	266.2	266.6	272.5	1.8	23.6	n.d.	4	0.215	0.322	4.25
141	269.1	268.8	272.6	2.0	24.5	n.d.	3	0.143	0.248	4.09
141	266.9	266.5	272.6	1.4	23.3	n.d.	4	0.151	0.230	3.84
L = 15 mm										
142	270.9	270.4	272.7	2.3	27.1	n.d.	5	0.088	0.175	4.19
200	267.0	267.2	272.9	2.7	24.9	n.d.	7	0.185	0.288	4.04
159	271.4	270.3	273.0	2.2	23.0	n.d.	n.d.	0.098	0.202	3.46
150	269.6	275.8	272.9	4.6	25.3	n.d.	10	0.130	0.234	3.93
L = 20 mm										
145	268.1	268.0	273.5	3.7	19.5	n.d.	n.d.	0.157	0.254	2.96
142	271.2	269.9	273.2	3.4	21.1	n.d.	4	0.099	0.201	3.15
150	273.0	271.5	273.3	3.5	21.7	n.d.	n.d.	0.049	0.127	3.18
142	269.0	267.8	273.4	2.7	22.3	n.d.	10	0.131	0.225	3.05
148	269.7	268.8	273.1	3.9	22.3	n.d.	n.d.	0.108	0.193	2.98
142	269.2	268.3	272.9	1.3	10.4	n.d.	12	0.086	0.141	2.76
L = 30 mm										
141	268.2	267.8	272.9	5.5	20.4	n.d.	11	0.121	0.199	2.56
141	269.6	269.1	272.4	1.3	10.8	n.d.	14	0.063	0.107	2.75
141	273.6	272.2	272.7	1.6	12.0	n.d.	16	0.027	0.077	2.52
141	269.4	269.4	273.0	1.4	9.7	n.d.	16	0.062	0.104	2.35
L = 40 mm										
141	271.7	271.4	273.3	1.6	7.4	20	45	0.036	0.073	2.16
141	269.8	270.0	272.9	1.7	7.6	25	46	0.048	0.082	2.20
121	267.9	268.0	272.8	1.3	6.9	n.d.	46	0.052	0.079	2.15
141	269.4	268.9	272.7	1.3	6.7	18	42	0.050	0.083	2.12
L = 50 mm										
142	269.6	270.5	272.6	1.6	4.4	31	75	0.052	0.087	1.74
142	270.2	270.6	272.7	1.4	4.6	24	90	0.039	0.068	1.91
203	271.1	271.4	272.8	2.4	6.8	22	95	0.018	0.034	2.29
L = 60 mm										
242	270.3	270.6	272.4	3.1	9.3	29	140	0.023	0.040	2.08
246	270.5	270.1	272.4	4.2	11.5	18	140	0.022	0.040	2.18
241	272.8	273.0	272.6	2.8	7.4	26	140	0.013	0.030	2.19
L = 75 mm										
411	271.2	271.1	272.9	1.5	6.1	60	200	0.018	0.033	2.32
399	271.2	271.6	272.1	3.4	10.4	n.d.	n.d.	0.012	0.023	2.55
441	271.1	271.2	272.5	2.6	8.5	35	230	0.015	0.028	2.41

[a] L is the thickness of regolith on top of the ice.
[b] Data averaged on the estimated steady state portion of the mass loss curves (see Section 3.2).
[c] Last temperature measured.
[d] Transition times on the mass loss curves as defined in the Section 3.2 (t_1: transition to adsorption and t_2: time to reach steady state).
[e] Rough sublimation rate calculated from the steady state slopes.
[f] The error on the steady state slope is about 6×10^{-4} mm h^{-1} or 0.8% of the E_S value.
[g] Sublimation rate calculated for standard temperature and relative humidity (273 K and 10 Pa) and corrected for the effect of bulk transport or advection, using Eq. (5).

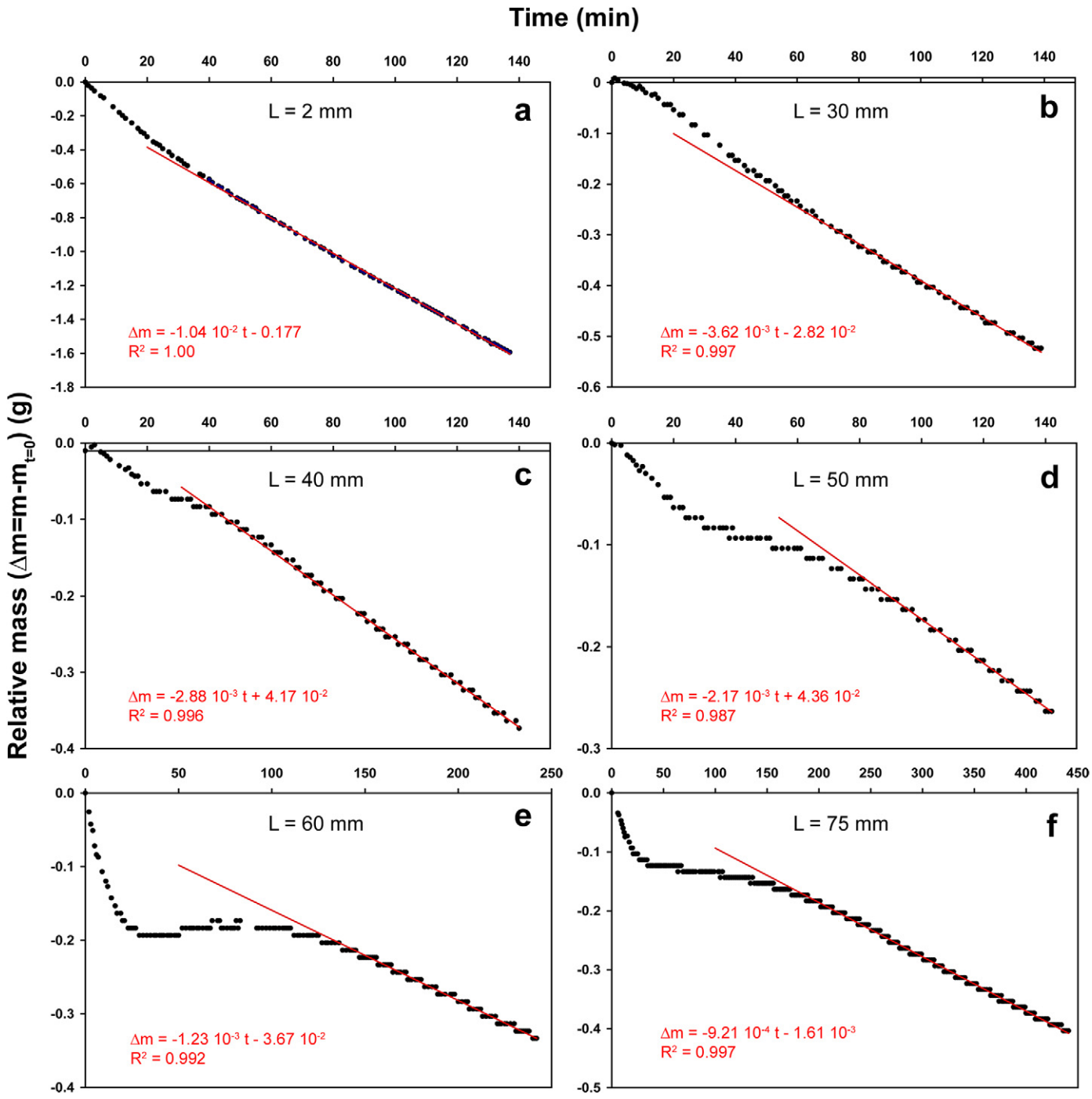

Fig. 2. Examples of our experimental data. The mass of the sample, relative to its starting mass, is plotted as a function of time for each of six depths of clay. The rapid early decay represents the loss of water and carbon dioxide adsorbed in the clay before the experiment began. This is more significant for greater depths of clay. The horizontal portion reflects a period during which water vapor leaving the ice is adsorbed onto the clay particles and does not leave the sample. This is also particularly important for greater depths of clay. The final, linear portion of the curves represents a period when steady state has been achieved and water vapor is passing through the clay at the rate it is leaving the ice. The regression line and R^2 value for this portion of the curve is indicated on the plots.

3.3. Temperature dependence of sublimation rate

In addition to clay layer thickness, the sublimation rate of the ice is also dependent on temperature (Chevrier et al., 2007; Sears and Chittenden, 2005). In Fig. 7 we plot the sublimation rates as a function of temperature for various clay layer depths. We use the conventional meteorological unit for evaporation and condensation, namely mm h^{-1}, which can easily be calculated from g min^{-1}. Four observations can be made from this figure.

First, the clay layers reduce the sublimation rate well below the value for exposed ice at every temperature investigated. Second, there is a decrease from 2.27×10^{-1} mm h^{-1} (at 263.5 K) to 1.81×10^{-2} mm h^{-1} (at 271 K) in the sublimation rate as the

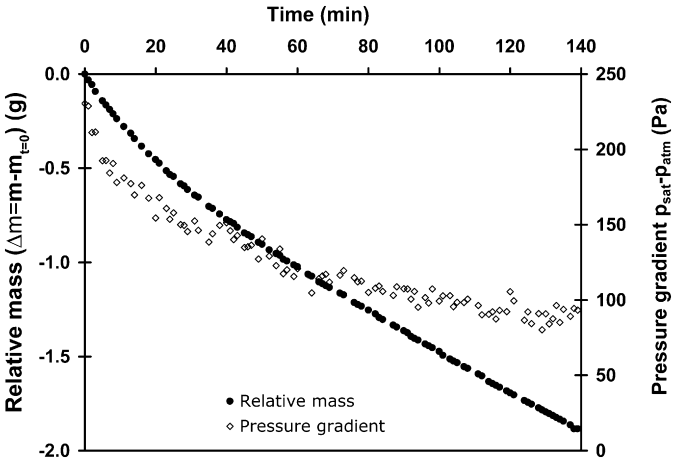

Fig. 3. The mass of the sample, relative to its starting mass, plotted as a function of time compared with the water vapor pressure gradient (the difference in the saturated vapor pressure and atmospheric pressure), which is a measure of inverse humidity. These data were generated with a 2 mm deep layer of clay, the run during which the highest relative humidities were reached (35%). The data show the dependence of evaporation rate (i.e. mass loss) and humidity (which increases downward on this plot).

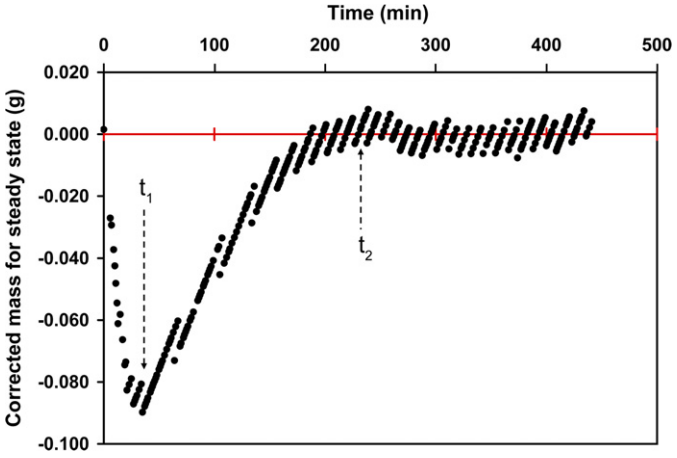

Fig. 4. The data in Fig. 2f ($L = 75$ mm) with the steady state loss subtracted. Plots like this better enable the times t_1 and t_2 to be identified. t_1 is the time to settle down, the time at which water and carbon dioxide adsorbed at 1 atmosphere during the set-up process are released. t_2 is the time at which the clay has adsorbed its full uptake of evaporating water vapor after which evaporating water passes straight through the clay layer.

thickness of the clay layer increases from 2 to 75 mm. Third, there appears to be no pronounced dependence of sublimation rate on temperature for a given clay depth because our temperature range is too small, only 3–4 K for a given depth. Fourth, there is a tendency for temperature to decrease with decreasing thickness, presumably due to evaporative cooling. Since the heat transfer from the atmosphere is very slow, the latent heat for sublimation is provided by the ice and clay which are therefore cooled down. This effect is less for larger depths of clay because they are a larger energy reservoir. Therefore, the usual decrease in mass loss rate with thickness is balanced by the increase of surface temperature with increasing thickness. From 2 to 75 mm, the sublimation rate should decrease by a factor ∼38 (see Section 4.1), while the temperature difference generates an

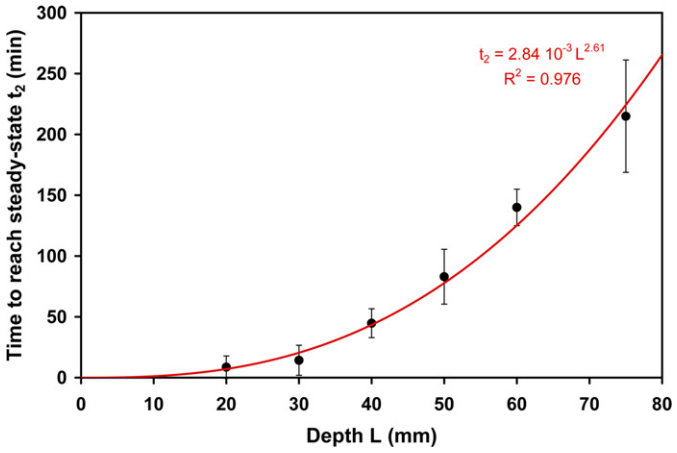

Fig. 5. Time to reach steady state, t_2 (see Fig. 4), as a function of the depth of the regolith, L. The curve and equation correspond to an empirical power fit to the data.

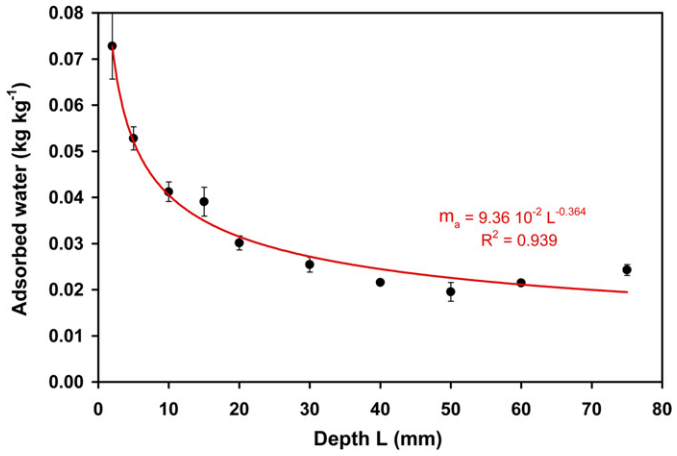

Fig. 6. Adsorbed water as a function of depth under steady state conditions. The curve and equation are an empirical fit to the data. The shape of this curve is determined by changes in surface temperature and humidity caused by changes in the depth of the overlying clay layer.

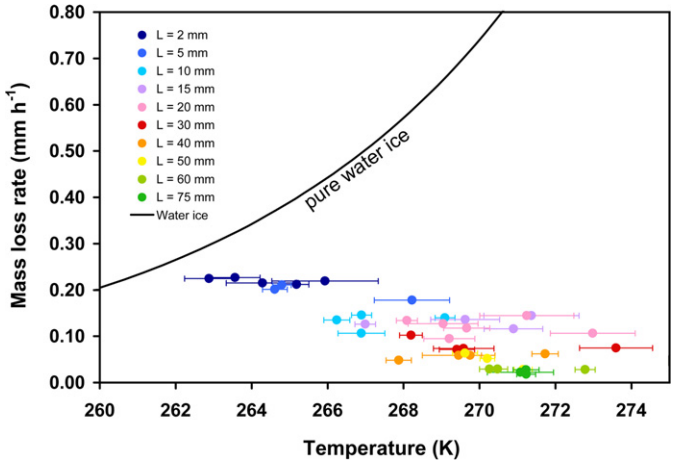

Fig. 7. Sublimation rate, E_S (determined from the steady state slopes identified in Fig. 2), as a function of surface temperature for a variety of clay depths, L. The data lie below the theoretical (Ingersoll, 1970) and experimental (Moore and Sears, 2006) curve for water ice sublimation. Sublimation rate decreases with regolith thickness. Also apparent is a decrease in the surface temperature with decreasing clay depth, which results from evaporative cooling.

increase by a factor 2.3. This results in a global decrease of sublimation rate by a factor 16, which is very close to the decrease observed in the data (a factor ∼13).

4. Discussion

We will discuss our data in terms of the diffusion of water vapor through clay layers, the adsorption of water vapor on the clay, and then describe a treatment that deals with the simultaneous diffusion and adsorption of water vapor passing through a clay layer. Finally we will discuss the implications of our work for two issues of importance in water behavior on Mars, the stability of subsurface ice and the role of clay in the diurnal water cycle.

4.1. Steady state diffusion and diffusion coefficients

Under steady state diffusion conditions there is an inverse relationship between the flux of water molecules and the thickness of the regolith layer. Such a relationship was theoretically described by Farmer (1976) and experimentally observed for the Mars soil simulant JSC Mars-1 by Chevrier et al. (2007). Under these conditions we can write:

$$J = \frac{DM_{\mathrm{H_2O}} p_{\mathrm{sat}}}{RT_S L}, \tag{1}$$

where J is the flux of water vapor molecules (in $\mathrm{kg\,m^{-2}\,s^{-1}}$), $M_{\mathrm{H_2O}}$ is the molecular weight of water, R is the ideal gas constant, T_S is the ice surface temperature, L is the thickness of the regolith layer and p_{sat} is the saturation pressure of water ice at temperature T_S, calculated using an empirical fit of the CRC Handbook of Chemistry and Physics (1995–1996 edition) data:

$$\log\bigl(p_{\mathrm{sat}}(\mathrm{bars})\bigr) = 7.551 - \frac{2666}{T_S}. \tag{2}$$

The temperature is assumed to be homogeneous across the clay layer. In terms of evaporation rate (in $\mathrm{m\,s^{-1}}$ or more frequently in $\mathrm{mm\,h^{-1}}$), Eq. (1) becomes:

$$E_S = \frac{DM_{\mathrm{H_2O}} p_{\mathrm{sat}}}{LRT_S \rho_{\mathrm{ice}}}. \tag{3}$$

This equation assumes a completely dry atmosphere, but it can be modified to include the water vapor present in the martian atmosphere as well as the temperature difference between the atmosphere and the surface of the sample. Thus:

$$E_S = \frac{DM_{\mathrm{H_2O}} p_{\mathrm{sat}}}{LRT_S \rho_{\mathrm{ice}}}\left[1 - \frac{T_S p}{T_{\mathrm{atm}} p_{\mathrm{sat}}}\right] \tag{4}$$

in which p and T_{atm} are the water vapor pressure and temperature of the atmosphere, respectively. As in our earlier work (Bryson et al., 2008; Chevrier et al., 2007), we use this equation to calculate the mass loss rates at 273 K and a humidity of 10 Pa of water from our experimental measurements (Table 2), and in this way remove scatter caused by varying temperatures and humidities.

Since the sublimation of ice creates an active source of water, in addition to transport by diffusion there will be a global movement of water by what is normally termed advection. Advection becomes significant when the molar fraction of water becomes significant compared to the total gas density; in our case this is achieved when the partial pressure of water becomes close to the total pressure, i.e. at temperatures close to 273 K. Analysis of the advection process shows that the ratio of both diffusive and diffusive plus advective fluxes is equal to (R. Ulrich, personal communication):

$$\frac{E_{S,\mathrm{Adv}}}{E_S} = \frac{\ln[\frac{1-p/P}{1-p_{\mathrm{sat}}/P}]}{p_{\mathrm{sat}}/P - p/P}, \tag{5}$$

where $E_{S,\mathrm{Adv}}$ is the sublimation rate including the advection term, E_S is the sublimation rate for pure diffusion (Eq. (4)) and P is the total atmospheric pressure. We used Eq. (5) to correct all measured for the advection effect, and thus have only diffusive flux. We found that, due to our high temperatures and high humidity, the sublimation rates calculated without taking count of the advection were 1.8 ± 0.3 times than their purely diffusive counterparts.

Diffusive sublimation rates are plotted as a function of soil depth in Fig. 8a. The large error bars at shallow depth are due mainly to the uncertainties in the thickness of the clay layer. Irregularities on the surface and difficulties in estimating this thickness result in an uncertainty of ∼1 mm which generates an uncertainty of about 25% in the sublimation rate in the 2 mm depth region. Moreover, both 2 and 5 mm experiment show very high humidities, 25–35% (Table 2).

The slope of a plot of sublimation rate against the inverse of the clay layer thickness yields the diffusion coefficient for water vapor diffusing through the clay. This plot is shown in Fig. 8b. With the exception of the data for the shallowest depths, 2 and 5 mm, we see a linear relationship consistent with steady state conditions and with sublimation being governed by diffusion of water vapor through the clay layer. From this we obtain a diffusion coefficient of $1.08 \pm 0.04 \times 10^{-4}\ \mathrm{m^2\,s^{-1}}$.

At shallow depths the sublimation rate no longer seems to be solely dependent on diffusion through the clay but, as previously discussed by Chevrier et al. (2007), diffusion through the atmosphere becomes also important. We can describe the data in a way that includes the shallow depths by the following semi-empirical relationship:

$$E_S = \frac{E_0 BL^{-1}}{1 + BL^{-1}}, \tag{6}$$

where E_0 is the sublimation rate of pure ice in the absence of a clay layer and:

$$B = \frac{DM_{\mathrm{H_2O}} p_{\mathrm{sat}}}{RT_S \rho_{\mathrm{ice}}}\left[1 - \frac{T_S p}{T_{\mathrm{atm}} p_{\mathrm{sat}}}\right] \tag{7}$$

in which E_S tends to E_0 as L tends to zero, and E_S tends to the steady state value given in Eq. (4) as L exceeds 10 mm. The average diffusion coefficient is then extracted from the value of B, using $E_0 = 1.14\ \mathrm{mm\,h^{-1}}$ (Fig. 8b). We obtain $D = 1.29 \pm 0.06 \times 10^{-4}\ \mathrm{m^2\,s^{-1}}$. This value is close to the value we obtained by a simple regression line on the points at $L \geqslant 10$ mm ($D = 1.08 \pm 0.04 \times 10^{-4}\ \mathrm{m^2\,s^{-1}}$).

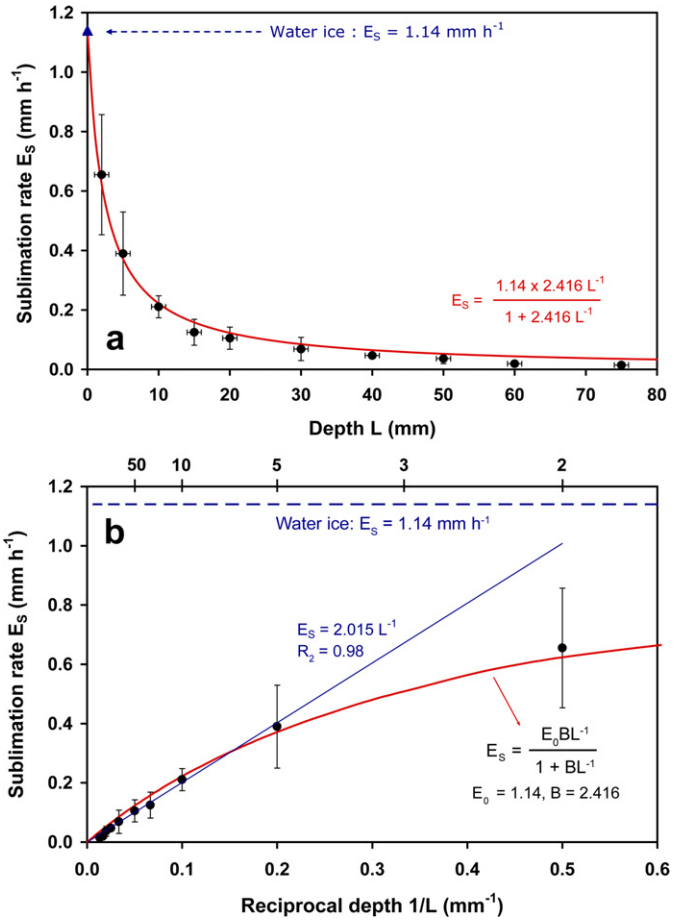

Fig. 8. (a) Sublimation rate, E_S, as a function of depth, and (b) sublimation rate as a function of reciprocal depth. The sublimation rate for pure water ice on Earth ($E_0 = 1.14$ mm h^{-1}) is indicated as a point of reference. Empirical fits to the data are indicated with the derived quantities. Fig. 8a simply describes the observations, with the regression line calculated from Eq. (6). Fig. 8b is an attempt to derive diffusion coefficients using Eq. (3) for the linear portion below 10 mm, when diffusion through the clay layer is the only rate determining process (thick solid line), and Eq. (6) which combines diffusion through the atmosphere as well as diffusion through the dust layer (thin solid line).

Most models of the advance and recession of an ice table and the simultaneous growth of a regolith on originally exposed ice have to deal with the problem of the ice-regolith discontinuity. This discontinuity results from the tendency of Eq. (1) to infinite flux when the layer of regolith tends to zero. Therefore, most models suppose a pre-existing regolith layer on top of the ice to solve the problem (Schorghofer, 2007). Equation (6) solves this problem by allowing the flux to tend to a zero regolith sublimation rate (E_0) that can be described by any adequate theory such as the Ingersoll equation (Ingersoll, 1970; Moore and Sears, 2006; Chevrier et al., 2007). Equation (6) could allow ice to be originally on top of the regolith. This could be highly important on Mars since sublimation is very dependent on the details of heat transfer between the atmosphere and the ice surface. Such heat transfer would be strongly modified if a regolith layer is preexisting or not on the ice.

The present determinations of the diffusion coefficient for water vapor through clay are similar to those previously obtained for other materials. Chevrier et al. (2007) obtained $1.74 \pm 0.70 \times 10^{-4}$ m^2 s^{-1} for the JSC Mars-1 palagonitic soil simulant. Bryson et al. (2008) obtained a value of $2.50 \pm 0.84 \times 10^{-4}$ m^2 s^{-1} for a layer of <63 μm basaltic grains. Hudson et al. (2007) found similar values for other materials, although our values are at the lower end of his range for similar grain size and porosity.

These experimental values show significant differences with theoretical estimates determined from grain size, porosity and tortuosity (Smoluchowski, 1968). We measured the porosity of our clay layers to be 0.66 (by normalizing the density of the regolith to the density of pure montmorillonite). In this case, according to Smoluchowski (1968) the tortuosity is about 3–4 and the theoretical diffusion coefficient is 3.83×10^{-4} m^2 s^{-1}, a value about 3–4 times our experimentally determined coefficients. Our lower value probably results from a higher tortuosity (around 10) most probably linked to the flat shape of clay particles and a broad range of particle size, both resulting in a more complex geometry.

In general we can conclude that, at least for the greatest part of natural unconsolidated regolith grain sizes, the diffusion coefficient remains in the range 10^{-4}–10^{-3} m^2 s^{-1}, especially since larger grain sizes induce larger pore sizes and thus result in larger diffusion coefficients (Bryson et al., 2008; Hudson et al., 2007; Smoluchowski, 1968). Moreover, a small number of large pores will control the transport process and this is probably the situation in most unconsolidated regoliths (Clifford and Hillel, 1983).

Knowing the diffusion coefficient we can estimate the time to reach steady-state, t_{SS}, for a pure diffusion process, since:

$$t_{SS} \approx \frac{L^2}{4D}. \tag{8}$$

Assuming our lowest estimate of the diffusion coefficient (i.e. $D = 1.08 \times 10^{-4}$ m^2 s^{-1}) and the largest clay layer thickness (i.e. 75 mm) we obtain $t_{SS} = 13$ s. Such time is not only far below the t_1 values (Fig. 5, Table 2) which average 26 min, but also far below the time resolution of our experiments. This suggests that a second phenomenon, namely adsorption, affects the timescales of the process, but not its amplitude (i.e. the diffusion coefficient does not change).

4.2. Adsorption

The shapes of our mass loss curves, summarized in Fig. 2, indicate that water vapor adsorption as well as diffusion will be important in regolith–water vapor interactions on Mars. There has been previous work on this topic; both theoretical (Houben et al., 1997; Jakosky, 1983, 1985; Jakosky et al., 1997; Zent et al., 1993) and experimental (Anderson et al., 1967; Fanale and Cannon, 1971; Zent and Quinn, 1995, 1997; Zent et al., 2001). Many materials can store substantial amounts of water at the low temperatures of Mars, and this is especially true for clays, which were recently identified in abundance on the south crust of Mars (Poulet et al., 2005).

Understanding the effect of adsorption on the transport of water vapor and the stability of ice requires the determination of thermodynamic constant α, and the kinetic coefficients of

adsorption k_a and desorption k_d. These are determined through the use of adsorption isotherms, which depend on the nature of the material (the abundance of adsorption sites, the relative adsorption and desorption energies) and on its surface area, which is ultimately related to grain size and porosity.

Chevrier et al. (2007) found that the palagonitic Mars soil simulant JSC-Mars 1 displayed a linear relationship between the desorption rate and depth, suggesting that the Langmuir theory was accurately describing the adsorption of water. This, in turn, suggests that the water was a monolayer, which is reasonable under the dry conditions in our experiments and those expected on Mars (Zent et al., 2001). The Langmuir isotherm is the following:

$$\theta = \frac{\alpha p}{1 + \alpha p}, \tag{9}$$

where θ is the fractional coverage of the monolayer, and α is the adsorption constant. The conversion from adsorbed mass m_a (in $\mathrm{kg\,kg^{-1}}$) to surface coverage is possible using the formula:

$$m_a = \theta \rho_{\mathrm{H_2O}} A_S l, \tag{10}$$

where $\rho_{\mathrm{H_2O}}$ is the density of the liquid water (1000 $\mathrm{kg\,m^{-3}}$), A_S is the specific area of the regolith and l is the thickness of the adsorbed monolayer (3×10^{-10} m for water). We used the relative humidity of the chamber to determine the pressure of water.

A plot of $1/\theta$ vs $1/p$ is shown in Fig. 9a. Instead of a single linear trend, we observe a break at 100 Pa and the slope above this pressure is about ten times the slope below this value. For the low-pressure line we determined the constant α and the surface area A_S, ensuring that θ has a value of 1 at infinite pressure (e.g. Eq. (9)). We obtained $A_S = 1.10 \pm 0.2 \times 10^5$ $\mathrm{m^2\,kg^{-1}}$ and $\alpha = 4.9 \pm 1.0 \times 10^{-2}$ $\mathrm{Pa^{-1}}$.

The data obtained at higher pressure show θ values lower than expected, indicating that we have more than one monolayer of water molecules on the clay particles. In this case the classic BET equation is applicable which can take the form (Brunauer et al., 1938):

$$\frac{p}{v(p_{\mathrm{sat}} - p)} = \frac{1}{v_m c} + \frac{(c-1)}{v_m c}\frac{p}{p_{\mathrm{sat}}}, \tag{11}$$

where p_{sat} is the saturation pressure of water, v is the adsorbed volume, v_m is the volume of one monolayer and c is the adsorption constant. In this case, we restricted the data range to data between 269 and 273 K, because it reduces the scatter on the data, puts an emphasis on the data with higher precision, and minimizes complications caused by temperature gradients between the surface and the atmosphere observed at lower temperatures. The result of applying the BET equation is shown in Fig. 9b. We confirmed that the parameters obtained on the restricted dataset were consistent with those on the full dataset within the uncertainties on the regression. Therefore, the BET model describes very well the adsorption of water on montmorillonite, in accordance with previous studies (Mooney et al., 1952). From the regression line we calculated the volume of the monolayer $v_m = 2.69 \pm 0.12 \times 10^{-5}$ $\mathrm{m^3\,kg^{-1}}$ and the BET adsorption constant $c = 30 \pm 10$. From the volume of the monolayer we calculate the specific surface area as

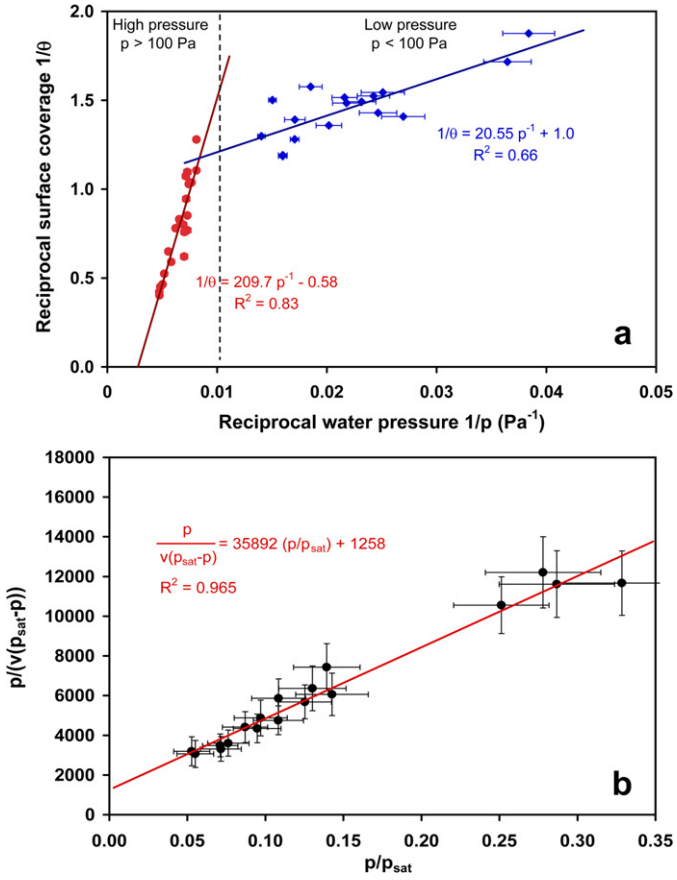

Fig. 9. (a) Adsorption data plotted on the assumption that the process can be described by the Langmuir isotherm which assumes a monolayer of water molecules on the surface of the clay grains. This discontinuity at 100 Pa indicates that the Langmuir isotherm only applies below this pressure. The line through the low pressure data is adjusted so that coverage is complete at infinite pressure. (b) On the other hand, all the data seem to be consistent with the BET isotherm, which is an extension of the Langmuir isotherm to allow for multiple layers of water molecules on the clay grains.

$A_S = 9.0 \pm 0.7 \times 10^4$ $\mathrm{m^2\,kg^{-1}}$. This value is similar to that determined from the Langmuir equation ($A_S = 1.1 \pm 0.2 \times 10^5$ $\mathrm{m^2\,kg^{-1}}$).

The value c is a function of the temperature (Brunauer et al., 1938):

$$c = \exp\left(\frac{E_1 - E_C}{RT}\right), \tag{12}$$

where E_1 is the latent heat of adsorption of the first layer, and E_C is the latent heat of adsorption of each subsequent layer, and so the latent heat of condensation (i.e. when the number of water molecules layers becomes too large, this is equivalent to a interstitial liquid). Thus we determined $E_1 - E_C = 7.6 \pm 1.6$ $\mathrm{kJ\,mol^{-1}}$. Equation (12) enables us to calculate the adsorption constant c at various temperatures, and from this we can calculate the corresponding isotherms. These appear in Fig. 10a. As expected, our data agree with the prediction of the Langmuir isotherm below 100 Pa and with the BET isotherms above 100 Pa. Moreover, nearly all the data plot between 263 and 273 K BET isotherms, in accordance with our measured temperatures.

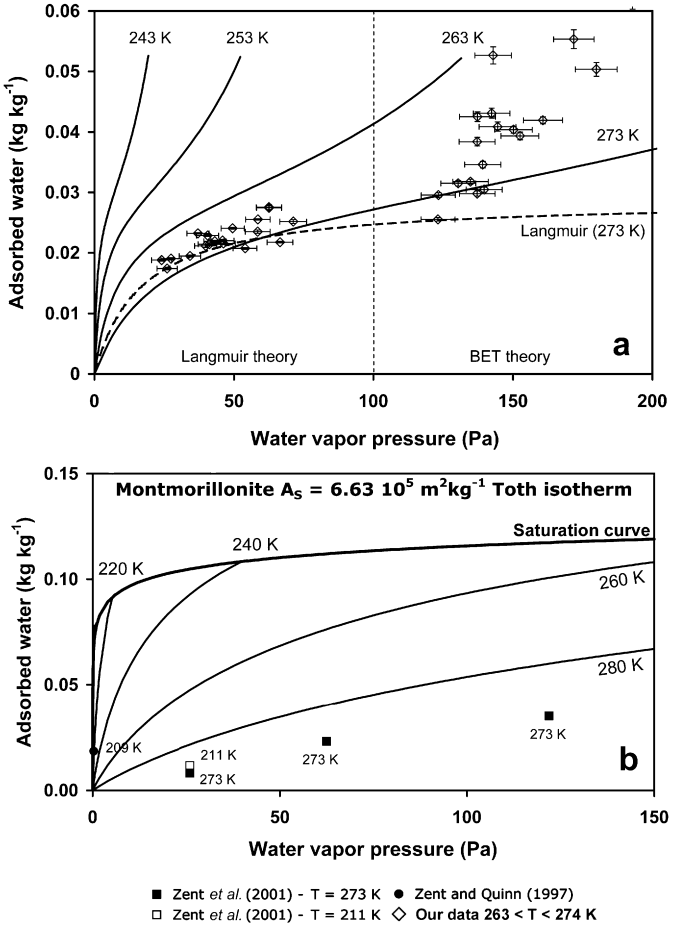

Fig. 10. Isotherms for water adsorbing onto clay particles derived from the present experiments compared with experimental data from the present and earlier studies. (a) Isotherms determined from our data, using both the Langmuir theory at 273 K (dashed line) and the BET theory at various temperatures (solid lines). The limit of application of the Langmuir theory (100 Pa) is indicated as a vertical dashed line. The diamonds represent the present data with their experimental uncertainties. (b) Isotherms determined by Zent and Quinn (1997), using the Toth theory and the specific surface area $A_S = 6.63 \times 10^5$ m^2 kg^{-1}. Are also presented the data used by Zent and Quinn (1997) for the determination of the isotherm, and later data obtained by Zent et al. (2001). The thick black line labeled "saturation curve" corresponds to the formation of the liquid phase. Although the amount of adsorbed water is very similar between both sets of experiments, the surface area of Zent's clays is about 6 to 7 times larger than ours. This suggests differences in grain size and/or effect of CO_2 adsorption in our experiments.

In Fig. 10b we compare our data with those of Zent et al. (2001) and Zent and Quinn (1997). We observe a similar content of adsorbed water, but the surface area measured by Zent and his colleagues for their clay samples was 6.63×10^5 m^2 kg^{-1}, about 6.5 times our value. Similarly Mooney et al. (1952) calculated a surface area for montmorillonite of $\sim 4.2 \times 10^5$ m^2 kg^{-1}. In addition to variations in grain size distribution, such difference in surface area could be due to adsorbed CO_2 in our experiments, as described in Section 3.1 (Zent and Quinn, 1995). CO_2 would occupy an important part of the surface area, decreasing the available surface for water. Since the majority of the atmosphere is composed of CO_2, the fact that the majority of the available surface area is occupied by CO_2 is not surprising. Further work will precisely quantify the relative adsorption of CO_2 and water in our experimental conditions.

4.3. Treatment of simultaneous diffusion and adsorption

Previous experimental work on the diffusion process for water vapor moving through the Mars regolith has neglected the interaction between the evaporating water and the surrounding porous material, while previous measurements of adsorption have been in static systems. Adsorption strongly affects the dynamics of the transport of water vapor, since it changes the pressure in the pores of the regolith. The differential equation accounting for both diffusion and adsorption processes is

$$\frac{\partial C_g}{\partial t} = \frac{\partial D}{\partial z}\frac{\partial C_g}{\partial z} + D\frac{\partial^2 C_g}{\partial z^2} - \frac{\partial C_a}{\partial t}, \tag{13}$$

C_g being the water vapor concentration in the regolith, and C_a the concentration of adsorbed molecules on the surface of the particles (Jakosky, 1985). This equation contains also the term $\partial D/\partial z$ accounting for a potential variation of D linked to changes in grain size, porosity, tortuosity, temperature, etc. This equation can be simplified into:

$$\frac{\partial C_g}{\partial t} = D'\frac{\partial^2 C_g}{\partial z^2}, \tag{14}$$

where

$$D' = \frac{D}{1 + \frac{\partial C_a}{\partial C_g}}. \tag{15}$$

$\partial C_a/\partial C_g$ is the slope of the isotherm at the corresponding conditions of pressure and temperature and D is the absolute diffusion coefficient. It is apparent from Eq. (15) that while the diffusion coefficient D remains constant, the adsorption process results in an apparent decrease of the diffusion coefficient described by the term $\partial C_a/\partial C_g$.

At martian surface pressures where pressure is well below 100 Pa we can apply the Langmuir equation. We can write the following adsorption rate R_a:

$$R_a = k_a(1-\theta), \tag{16}$$

where k_a is the adsorption kinetic constant. Similarly, the desorption rate R_d is

$$R_d = k_d\theta \tag{17}$$

with k_d being the desorption constant. Both kinetic constants k_a and k_d are related to the adsorption constant α through:

$$\alpha = \frac{k_a}{pk_d}. \tag{18}$$

Combining both kinetic Eqs. (16) and (17) leads to the differential equation that drives the variation of the adsorbed population with time:

$$\frac{\mathrm{d}\theta}{\mathrm{d}t} = k_a(1-\theta) - k_d\theta. \tag{19}$$

Solving this equation with the initial condition $\theta_{t=0} = 0$ (Zent et al., 2001) gives:

$$\theta = \frac{k_a}{k_a + k_d}\left[1 - e^{-(k_a+k_d)t}\right]. \tag{20}$$

As t tends to infinity this equation tends to Eq. (9).

We can now investigate the effect of adsorption on the diffusion process. Equation (14) implies that equilibrium is achieved simultaneously for both diffusion and adsorption, i.e. that $\partial C_a/\partial t = 0$ when $\partial C_g/\partial t = 0$ so that the steady state slopes of the curves give the absolute diffusion coefficient (i.e. $D' = D$). However, if steady state is not reached, then the adsorption kinetics must be considered. Using Eq. (13) combined with Eqs. (10), (18) and (20) we obtain a differential equation for the transport of water vapor allowing for simultaneous diffusion and adsorption in the martian regolith:

$$\frac{\partial p}{\partial t}\left[1 + \Psi\frac{\partial \theta}{\partial p}\right] = \frac{\partial D}{\partial z}\frac{\partial p}{\partial z} + D\frac{\partial^2 p}{\partial z^2}. \tag{21}$$

The constant Ψ corresponds to the thermodynamic part of the adsorption process and is defined by

$$\Psi = \frac{RT_S\rho_{H_2O}\rho_{reg}A_S l}{M_{H_2O}}, \tag{22}$$

where ρ_{reg} is the density of the regolith. Ψ is mainly dependent on the properties of the regolith (specific surface area and density) and calculated values are generally comprised between 10^5 and 10^7 J m^{-3}. The term $\partial\theta/\partial p$ corresponds to the dynamic part of the adsorption process which, in the Langmuir theory, is given by

$$\frac{\partial \theta}{\partial p} = \frac{\alpha}{(1+\alpha p)^2}\left[1 + \left(\alpha p k_d t(1+\alpha p) - 1\right)e^{-k_d(1+\alpha p)t}\right]. \tag{23}$$

For a constant diffusion coefficient (i.e. homogeneous grain size, porosity, etc.), Eq. (21) becomes equivalent to Eq. (14):

$$\frac{\partial p}{\partial t} = \frac{D}{[1 + \Psi\frac{\partial\theta}{\partial p}]}\frac{\partial^2 p}{\partial z^2}. \tag{24}$$

Equation (23) has the advantage of being valid in both Langmuir and BET theories since the BET represents the extension of the Langmuir for more than one layer of adsorbed molecules. In fact, since the BET theory is dependent on the relative humidity, rather than the total water pressure in the case of the Langmuir equation (compare both isotherms), the BET constant c is equivalent to the product of the Langmuir constant and the saturation pressure, or $c = \alpha p_{sat}$. This relationship allows using the kinetic constants k_a and k_d in the BET theory.

Analysis of Eq. (23) shows that the adsorption phenomenon during diffusion is not trivial. There are three important terms (Fig. 11):

(1) The term α (or c in the case of the BET theory) represents the efficiency of the adsorption process, i.e. how much water can be adsorbed, which is related to the availability of surface sites. Increasing the value of α of a factor 10 changes $\partial\theta/\partial p$ by one order of magnitude (Fig. 11a). Therefore, higher α values imply increasing amount of water interacting with the surrounding regolith. This effect is even more important since regoliths with high α, such as clays, generally present also high values of specific surface area and Ψ. However, α does not affect the timescale of the adsorption process.

(2) The term k_d (and implicitly $k_a = \alpha p k_d$) represents the kinetics of the adsorption process, i.e. the rate of exchange of the molecules on the surface of the grains. Equation (18) shows that large values of α imply large values of k_a and small of k_d. High values of α (and k_a) will have a strong effect on the diffusion coefficient. Alternatively, high k_d will imply a small value of α and then a short time to reach steady state. However, for a constant α, the value of k_d influences the time to reach equilibrium (Figs. 11a and 11b). Increasing the value of k_d of a factor 10 changes $\partial\theta/\partial p$ of

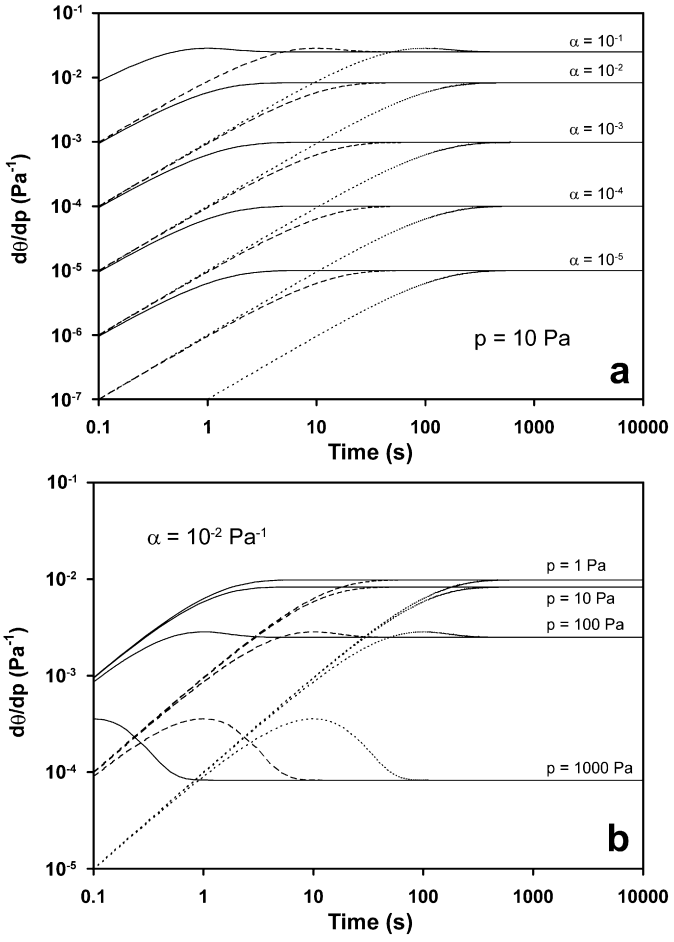

Fig. 11. Variation with time of $\partial\theta/\partial p$ (coverage variation with water pressure; this describes the adsorption of water on the surface of the montmorillonite grains, according to Eq. (23)) and assuming various relevant parameters. (a) Illustrates variation with the adsorption constant value α for 10 Pa of water pressure. (b) Illustrates the effect of various pressures for $\alpha = 10^{-2}$. In both (a) and (b), curves are shown for three values of desorption kinetic coefficient, k_d: 1.0 s^{-1} (solid lines), 0.1 s^{-1} (dashed lines) and 0.01 s^{-1} (dotted lines). The curves show that while α and p control the amplitude of the adsorption (how much water is adsorbed), the timescale of the adsorption is dependant on the kinetics constants k_a and k_d.

one order of magnitude. Thus our results suggest a high k_a and low k_d.

(3) The pressure is also an important parameter. Increasing the pressure by a factor 10 decreases $\partial\theta/\partial p$ by a factor 30 (Fig. 11b). The anticorrelation between $\partial\theta/\partial p$ and p is due to the lower number of available sites for water molecules at higher pressure. In other words, the effect of the adsorption on the diffusion process becomes less effective when the pressure tends to the equilibrium pressure. However, pressure affects the process in a much more complex manner since it is varying with time and depth.

Application of the previous coupled model requires the following parameters: D, α, k_a and k_d. With the steady state data we have been able to determine D and α. The determination of the kinetic constants k_a and k_d requires an analysis of the non-steady state portion of the curves, i.e. before t_2. Therefore, we selected data for kinetic analysis with the following characteristics: greater depth (so that adsorption is pronounced and the temperature gradient between the surface and the atmosphere is small) and constant pressure and temperature between the runs. We used the steady state slope curves adjusted to 273 K and 10 Pa. Then we assumed that diffusion and adsorption start at t_1. Finally, since we are concerned only with the kinetics of this process, we normalized the water mass to that determined at the end of the experiments.

Examples of the resulting calculations are shown in Fig. 12. Then, following Zent et al. (2001), we determined the least square fit to these data using Eqs. (10) and (20). We fixed the specific surface area to the value determined from the equilibrium analysis on the isotherms, i.e. $A_S = 1.09 \times 10^5$ m^2 kg^{-1} and the thickness of the monolayer to the same value, i.e. $l = 3 \times 10^{-10}$ m. The resulting values of k_a and k_d determined from the six analyses we performed are shown in Table 3. We obtain values remarkably uniform k_a and k_d values, with averages of $k_a = 2.5 \pm 0.5 \times 10^{-4}$ s^{-1} and $k_d = 8.7 \pm 3.6 \times 10^{-5}$ s^{-1}. We checked also the validity of our analysis by recalculating the value of the adsorption constant α using Eq. (18) (Table 3). All values are very close to the α value of 4.9×10^{-2} Pa^{-1} determined from the Langmuir isotherm, with the most extreme value being different by a factor less than 4. As expected we do not see any dependence of k_a or k_d in the small range of temperatures and pressures of our experiments.

To verify the validity of our model, equations and parameters, we numerically solved the diffusion equation (13) considering a constant diffusion coefficient (i.e. $\partial D/\partial z = 0$). We modeled the kinetics of adsorption using Eq. (20) and used the previously determined parameters: D, k_a, k_d and A_S. We used the numerical solver software COMSOL Multiphysics and applied the model to a 75 mm thick layer of regolith, considering 7 mbar of total pressure, homogeneous temperature of 273 K and zero atmospheric humidity, corresponding to our experimental conditions.

Results of the calculation show that instead of reaching equilibrium in a few seconds, according to Eq. (8), it takes about 250 min to reach steady-state, when both internal flux (ice to regolith) and external flux (regolith to atmosphere) become identical (Fig. 13a). The internal flux decreases strongly because of adsorption (Fig. 13a), while the external flux remains constant for about 120 min (Fig. 13b), which is the time to fill the regolith with water vapor. When the regolith reaches it maximum capacity for water adsorption, the external flux increases rapidly and reaches steady-state in about 250–300 min (Fig. 13b). The results of the calculations compare well with the experimental data (Fig. 13c), the small time difference between the data and the calculation (about 20–30 min) probably results from the fact that the kinetic constants k_a and k_d are determined after t_1 (time of initial mass drop, which falls in the range 20–30 min,

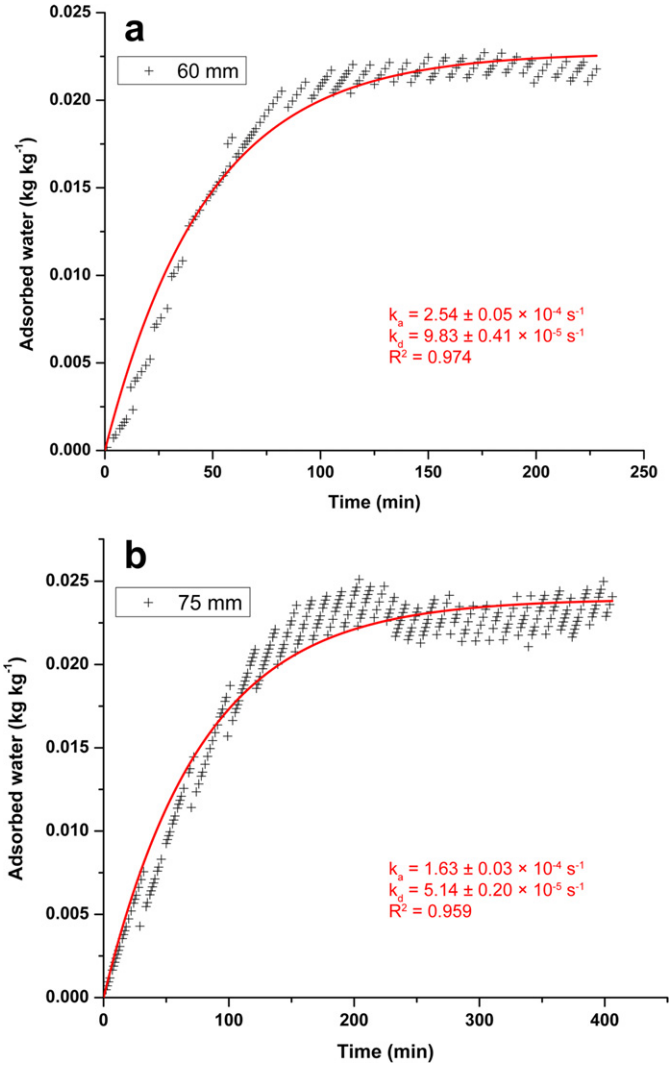

Fig. 12. Determination of kinetic data for adsorption assuming the Langmuir isotherm. The data have been corrected for steady-state diffusion, scaled at the time of diffusion start (t_1), and then normalized to the mass of water adsorbed, as measured at the end of the experiment. The solid curves correspond to the best fit determined using Eq. (20), and the following parameters: specific surface area $A_S = 1.09 \times 10^5$ m^2 kg^{-1} and thickness of the monolayer $l = 3 \times 10^{-10}$ m. Also indicated are the kinetic constants for adsorption (k_a) and desorption (k_d) with their uncertainties and regression coefficients, R^2. (a) Clay layer depth of 60 mm, water pressure $p = 57$ Pa and $T = 270.5$ K. (b) Clay layer depth of 75, in the following conditions: $p = 38$ Pa and $T = 271.1$ K (see also Figs. 2f and 4). Results are shown in Table 3. Averaged calculated values are $k_a = 2.5 \pm 0.5 \times 10^{-4}$ s^{-1} and $k_d = 8.7 \pm 3.6 \times 10^{-5}$ s^{-1}.

Table 3
Determination of adsorption kinetic constants k_a and k_d using the Langmuir theory

L (mm)	T_S (K)	p (Pa)	k_a (s^{-1})	k_d (s^{-1})	α[a] (Pa^{-1})
75	271.1	38	1.63×10^{-4}	5.14×10^{-5}	8.37×10^{-2}
60	270.3	47	2.12×10^{-4}	8.83×10^{-5}	5.11×10^{-2}
60	270.5	57	2.54×10^{-4}	9.83×10^{-5}	4.57×10^{-2}
60	272.8	36	2.51×10^{-4}	9.06×10^{-5}	7.63×10^{-2}
50	270.2	24	2.90×10^{-4}	1.46×10^{-4}	8.25×10^{-2}
50	271.1	31	2.99×10^{-4}	4.83×10^{-5}	1.98×10^{-1}
Average $\pm 1\sigma$			$2.5 \pm 0.5 \times 10^{-4}$	$8.7 \pm 3.6 \times 10^{-5}$	

[a] Calculated using Eq. (18).

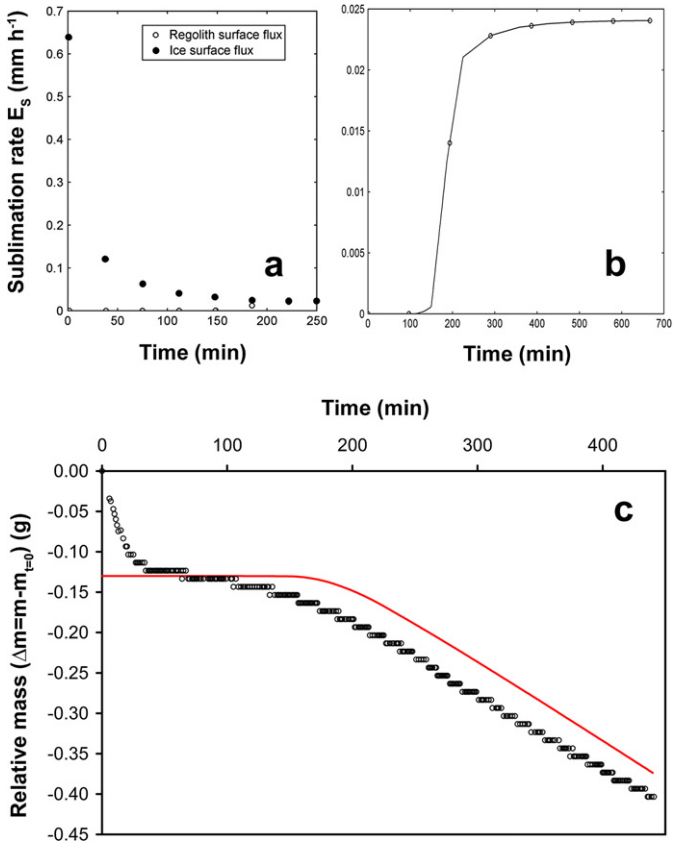

Fig. 13. Results of the numerical solution describing the model of simultaneous diffusion and adsorption applied to a 75 mm clay thick regolith, at 273 K and zero humidity, using equations described in Sections 4.2 and 4.3. We use the parameters determined in this study, i.e. $D = 1.08 \times 10^{-4}$ $m^2\,s^{-1}$, $A_S = 9.0 \times 10^4$ $m^2\,kg^{-1}$, $k_a = 2.5 \times 10^{-4}$ s^{-1} and $k_d = 8.7 \times 10^{-5}$ s^{-1}. (a) Black circles refer to water vapor flux at the ice–regolith interface and open circles refer to the water vapor flux at the regolith–atmosphere interface. (b) Details of the flux at the regolith–atmosphere interface, showing no flux for about 120 min, followed by a strong increase with steady state after about 250–300 min. (c) Comparison of the calculated flux (solid line) and the experimental data (open circles). Apart from the early 20–30 min, corresponding in majority to desorption of CO_2 and H_2O desorption during set-up. There is very good agreement between the calculated and observed fluxes.

see Table 2). This small drop of mass at the beginning of the experiment is related to desorption of CO_2 and H_2O from the regolith during set-up and is not accounted by the model. Thus our analysis, formulation of the problem and the parameters we derive from our experiments enable us to accurately predict the behavior of water in the regolith analog, and can be used in a variety of contexts in the our attempts to understand such processes on Mars during, for example, the diurnal cycle.

4.4. Implications for state and stability of water on Mars

4.4.1. Diffusion of water vapor through martian clay regolith and stability of subsurface ice

Smoluchowski (1968) theorized that regolith layers could protect ice layers from sublimation by providing a significant barrier to the diffusion of water vapor. However, this result requires very low diffusion coefficients, which we do not observe for our clay powder layers. Our measured diffusion coefficient of 1.29×10^{-4} $m^2\,s^{-1}$ indicates that water diffuses very fast in our clay regolith. With such diffusion coefficient, it is highly unlikely that the regolith will provide a significant protection to ice sublimation, especially when considering previous measured diffusion coefficients on various martian regolith analogues (JSC Mars-1, basalt, dust) that always fall in the range 10^{-4}–10^{-3} $m^2\,s^{-1}$ (Bryson et al., 2008; Chevrier et al., 2007; Hudson et al., 2007). Therefore, temperature remains the main factor stabilizing ice on the surface of Mars, and in most regions the presence of ice is possible only if the temperature is low enough. This result is nevertheless valid for shallow depth of unconsolidated regolith. Packing of the dust at higher depths strongly reduces the porosity and eventually decreases the diffusion rates of water vapor (Clifford and Hillel, 1983). However, such depths are probably out of the range of the GRS spectrometer. Other phenomena such as formation of thick duricrusts through alteration and eventually cementation by other salts (Jakosky and Christensen, 1986; Cooper and Mustard, 2002) may be effective at shallow depth and result in similar reduction of the diffusion process. These phenomena are nevertheless different from a loose superficial regolith and will be the object of further studies.

Surface temperatures can strongly vary according to the diurnal cycle but this variation is completely attenuated at depth of a few centimeters (Mellon et al., 2004; Schorghofer and Aharonson, 2005), while seasonal variations disappear at depth below 1 m. If the average temperature at this depth does not stabilize the ice, then it will continuously sublimate through any potential regolith showing similar diffusion coefficient to our measured value. In regions with average high temperatures, ice would be possible at shallow depth in only two cases: (1) if there is an exact balance between the amount of ice sublimated

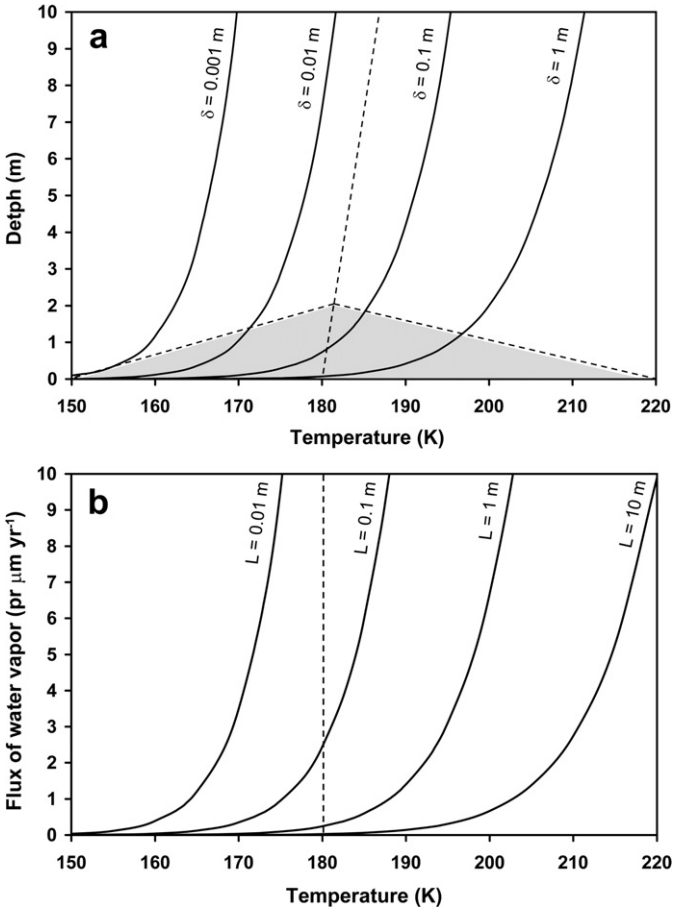

Fig. 14. Metastability of shallow ice on Mars. (a) Depth *versus* temperature necessary to have a layer of ice of thickness δ still present after 300,000 years. For our present purposes we consider that the regolith layer thickness remains constant. We use for the diffusion coefficient $D = 1.08 \times 10^{-4}$ m^2 s^{-1}. The gray area indicates temperature variations during the diurnal cycle (Mellon et al., 2004). The dashed vertical line represents the subsurface geotherm for an unconsolidated regolith (Mellon and Phillips, 2001). The gray area indicates the amplitude of the diurnal cycle below the surface. Any layer of thickness δ above its temperature vs depth curve will disappear in the time period of 300,000 years. The geotherm of 180 K indicates that only layers of thickness above 0.1 m would still be present at high latitudes. The gray area indicates that the stability of the corresponding layer would depend on the period of the day, even if ultimately only the average temperature is significant for the stability of ice, as shown by previous studies (Schorghofer and Aharonson, 2005). Alternatively, layers thinner than 0.1 m would be present in regions of lower temperature. (b) Amount of water vapor released in the atmosphere, in precipitable micrometers per year (pr μm yr^{-1}) as a function of the temperature for various thickness of regolith. The amount of released water vapor is usually below the observed humidity in the martian atmosphere, especially for layer shown to be stable at the average temperature in Fig. 14a. For example, a 1 m layer at 180 K still present today would release less than 0.5 pr μm yr^{-1} of water vapor. In these conditions shallow ice could be still present without generating large amounts of water vapor, especially if local sinks like polar caps or seasonal frost are present.

during the day and the amount condensed during the night, (2) if a mechanism acts as a buffer during ice sublimation.

There is a strong orbital forcing of the martian climate, related to the obliquity variations, which affects the ice stability and distribution (Head et al., 2002; Schorghofer, 2007). For the past 300,000 years Mars had been in a period where ice is globally transferred from the equatorial regions to the poles. Therefore the potential presence of ice in equatorial regions could be due to remnants of old ice still sublimating. Fig. 14a shows the required temperature and depth, calculated using Eqs. (4) and (6), in which metastable ice could exist in the shallow subsurface. Even thin layers of ice, below 1 m thick, can last 300,000 years in the upper few meters at the average high-latitude (∼65°) surface temperature of 180 K (Mellon et al., 2004). Water in the shallow subsurface at lower latitudes could be remnants of thick layers accumulated in the equatorial regions during periods of higher obliquity (Schorghofer, 2007), and still sublimating today. This would be especially the case if induration or cementation of the regolith occurred, resulting in much lower diffusion rates.

Ground based measurements and MGS-TES observations indicate variable amounts, from 10 to 20 pr μm (precipitable micrometers) of water vapor in the atmosphere of Mars (Smith, 2002; Sprague et al., 2006), with peaks to 100 pr μm in the North hemisphere and 50 pr μm in the South hemisphere (Smith, 2002). If sublimating, the ice layer may be in the shallow subsurface and produce very limited amounts of water vapor (Fig. 14b). Even at a 10 cm depth, the amount of water vapor produced does not exceed 4 pr μm per year. Therefore, if some remnants of equatorial ice are still sublimating today, the amount of released water vapor is the same order of magnitude as the atmospheric water vapor. Therefore, flux of water vapor from sublimation at low latitudes can be easily balanced by other sinks, and especially the polar caps, or seasonally, by frost.

4.4.2. *Adsorption of water vapor by a clay regolith and implications for the humidity diurnal cycle*

The second source of water in the subsurface is water vapor adsorbed on the surface of clay grains. Clays are strong water absorbers (Anderson et al., 1978; Mooney et al., 1952; Zent et al., 2001). The main parameter controlling the amount of water stored in the clay is the relative humidity in the atmosphere and the temperature. Therefore, changes in these two parameters should induce release or trapping of atmospheric water in the regolith. However, our study also shows that even if clays can store large amounts of water, their equilibration is slow. Using the empirical formula determined in Fig. 5, we calculate that any layer deeper than 12 cm will never react to any diurnal change in humidity and keep adsorbed water at longer timescales than one day and thus account for some of the water detected in the martian subsurface. According to our study, montmorillonite can store up to 8 wt% H_2O in high humidity. This value is very similar to the highest values observed in the equatorial regions of Mars (up to 12 wt%, Jakosky et al., 2005). The 8% value corresponds also to a high temperature (about 265 K), so at the average subsurface temperature of 220 K, the amount could be higher. Therefore, water in the equatorial regions could be adsorbed water in a clay regolith, provided the corresponding layer is thicker than 12 cm, which is very possible since GRS detects water down to about 1 m. In this case, this adsorbed water would be isolated from the atmosphere and not contribute to the diurnal cycle. If considering the seasonal vari-

ations of humidity, the equilibration layer for 3 martian months is about 1 m (using the same empirical equation in Fig. 5), once again in the GRS depth range. This means that higher seasonal humidity can be recorded in the shallow regolith and further detected by GRS. However, longer timescale variations in humidity will be easily reequilibrated with the atmosphere.

The average daily water content goes from about 10 to 40 pr μm (Smith, 2002; Sprague et al., 2003, 2006), while often the diurnal cycle shows variations of about 10–20 pr μm. Such variations could be due to the adsorption in the upper layer of the clay regolith (Jakosky et al., 1997; Flasar and Goody, 1976). During the night, when the temperature drops, a part of the daytime humidity gets adsorbed into the regolith. To have more precision on the conditions of adsorption of water in a clay regolith, we calculated the thickness of the adsorbent layer ε, as a function of the average temperature of the surface T_S, using the following formula:

$$\varepsilon = \frac{\Delta\xi}{\rho_{\text{reg}}\Delta v}, \tag{25}$$

where $\Delta\xi$ is the difference between night and day of atmospheric water vapor content in pr μm ($\Delta\xi = \xi_{\text{day}} - \xi_{\text{night}}$), Δv is the difference of adsorbed volume ($\Delta v = v_{\text{night}} - v_{\text{day}}$), calculated using the BET isotherm (Eq. (11)) and ρ_{reg} is the density of the regolith. Even if the Langmuir isotherm is perfectly accurate at martian water pressures ($p \ll 100$ Pa), the BET gives the dependency of the adsorption constant c with temperature (e.g. Eq. (12)), which is of primary importance in adsorption calculations, since there is a strong difference between surface night and day temperatures (Mellon et al., 2004; Schorghofer and Aharonson, 2005). The saturation pressure is calculated using Eq. (2) and the water vapor pressure in the atmosphere of Mars is calculated using the ideal gas law, in this case:

$$p = \frac{\rho_{\text{H}_2\text{O}}\xi RT}{M_{\text{H}_2\text{O}}h}. \tag{26}$$

h is the scale height of the atmosphere (between 7 and 11 km) and T is the temperature of the night or the day (minimum and maximum temperatures that borne the diurnal cycle). We assume a constant temperature across the air column and at the interface, which is only approximately true. However, the difference of surface temperature is the main parameter for adsorption, while the temperature of the atmosphere only slightly modifies the water vapor pressure in the atmosphere (Eq. (26)). The significant water vapor pressure is that at the regolith–atmosphere interface. Since the adsorption is driven by the diurnal cycle, the temperature amplitude ΔT was used to relate minimum (night) and maximum (day) temperatures to the average temperature T_S by the simple approximations: $T_{\text{night}} = T_S - \Delta T/2$ and $T_{\text{day}} = T_S + \Delta T/2$. Both night and day temperatures are used to calculate the pressure of water and the adsorption constant using Eq. (12).

Thus by using the previous equations and approximations we calculated the thickness of clay ε necessary to adsorb the atmospheric water vapor difference during the diurnal cycle as a function of the average surface temperature (Fig. 15). The first major conclusion to derive from Fig. 15 is that water vapor adsorption is favored in warmer regions, i.e. where temperature exceeds 200 K. Indeed, if adsorption efficiency strongly increases with lowering temperature, the saturation pressure also drops quickly (e.g. Eq. (2)). If the pressure of water in the atmosphere becomes higher than the saturation pressure ($p > p_{\text{sat}}$), which occurs around 200 K, the water condenses on the surface of the regolith, rather than being adsorbed. This phenomenon explains the formation of frost on Mars (Anderson et al., 1967) in the northern regions as observed by Viking Lander 2 (Hart and Jakosky, 1986; Wall, 1981), not because the regolith is not

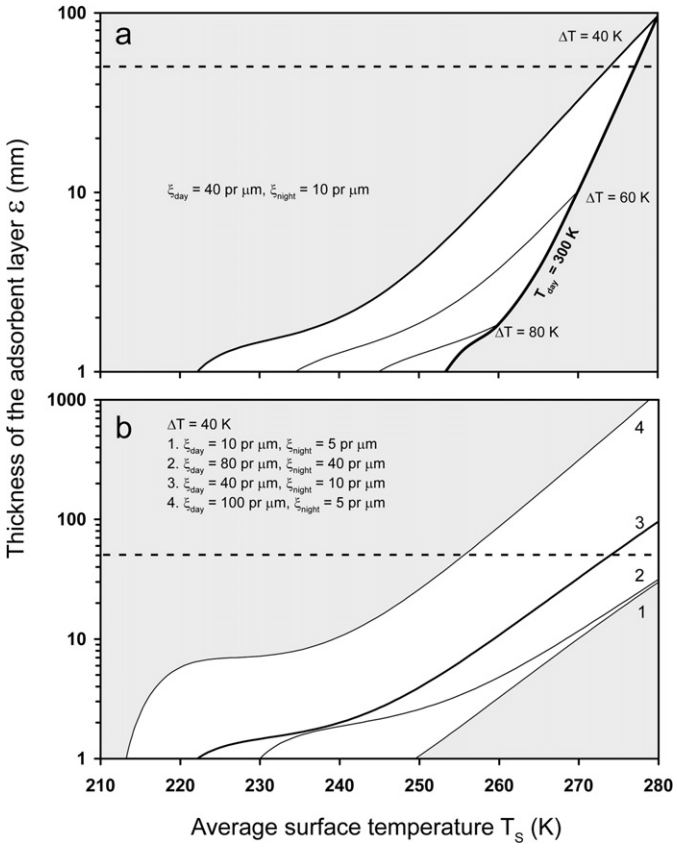

Fig. 15. Thickness of the absorbing clay layer, ε (in mm), as a function of the average surface temperature, T_S, calculated using the BET theory (Eqs. (11) and (12) and Eqs. (25) and (26)). We investigate also the two important parameters controlling the adsorbed water in the clay layer: the diurnal temperature cycle, ΔT, and atmospheric water content, $\Delta\xi$. The horizontal dashed lines indicate the diurnal thermal skin depth, arbitrary fixed here at 4 cm. (a) Dependency of the adsorbing thickness with the diurnal temperature variation ΔT. We consider the following diurnal water vapor variation: $\xi_{\text{day}} = 40$ pr μm and $\xi_{\text{night}} = 10$ pr μm. The thick black curve represents the maximum temperature reached on the martian surface, i.e. $T_{\text{day}} = 300$ K. The medium thick line represents the same model in figures (a) and (b) for comparison ($\Delta T = 40$ K, $\xi_{\text{day}} = 40$ pr μm and $\xi_{\text{night}} = 10$ pr μm, curve 3 in figure (b). (b) Variation with water vapor content of the atmosphere ξ. The temperature amplitude is $\Delta T = 40$ K. We use three models for comparison, a humid Mars, a dry Mars, and a Mars of extremes: model 2, $\xi_{\text{day}} = 80$ pr μm and $\xi_{\text{night}} = 40$ pr μm: model 3, $\xi_{\text{day}} = 10$ pr μm and $\xi_{\text{night}} = 5$ pr μm: model 4, $\xi_{\text{day}} = 100$ pr μm and $\xi_{\text{night}} = 5$ pr μm). The results show that unless extreme models (low temperature, extreme variations of humidity), the layer of clay required to adsorb the water vapor during the diurnal cycle is below the limit of clay reactivity of 12 cm determined using empirical relationship determined in Fig. 5.

adsorbing water, but because the saturation vapor pressure is far too low to allow adsorption. The average temperature at the Viking Lander 2 site is about 210 K (Hess et al., 1977), indicating that adsorption should be low, and the diurnal cycle could be rather described by direct condensation from atmospheric vapor. Therefore, adsorption in the regolith implies that the average temperature remains quite high. Similarly to the average temperature, the amplitude of the diurnal cycle is important, since on the one hand large amplitude causes low temperatures and frost formation, while on the other hand causing temperatures too high for adsorption. In the same time, large amplitudes increase the adsorption efficiency. Therefore, increasing the thermal amplitude during the diurnal cycle decreases the thickness of the layer adsorbing water but also the range of favorable temperatures (Fig. 15a).

Another important parameter to consider is the amount of atmospheric water in the atmosphere ξ. The absolute value is not as important as the amplitude of the variation. Curves 2 and 3 in Fig. 15b correspond to atmospheres with humidity eight times that of the curve 1. Large amplitudes for the water vapor change, $\Delta\xi$ (Fig. 15b), favors the maximum surface penetration. For all temperatures amplitudes, and nearly all atmospheric water variations considered, the thickness of the adsorbing layer is always below 12 cm, and below the diurnal thermal skin depth of about 4 cm. Only when using extreme values of humidity variations, i.e. from $\xi_{\text{day}} = 100$ pr µm to $\xi_{\text{night}} = 5$ pr µm (Smith, 2002), very small temperature amplitudes, and relatively high average temperatures, we find that layers up to 1 m can adsorb water in the warmest regions (above 260 K, Fig. 15b). Such models have very restrictive conditions, and in most cases shown in Fig. 15 the required thickness remains thinner than the thermal skin depth.

Applying this model to the Pathfinder Landing site, where the temperature is quite high, 230 K on average with and amplitude $\Delta T = 60$ K (Schofield et al., 1997) and a dry atmosphere with $\Delta\xi \sim 10$ pr µm (Smith et al., 1997) shows that a very thin layer of clays (<1 mm) could largely adsorb all the water during the diurnal cycle. Moreover, the clays can also be dispersed in a regolith of different mineralogy and still act as an efficient adsorbent. Since clays have been highly impacted due to their Noachian origin (Poulet et al., 2005), it is probable they are well dispersed on the surface of Mars. Therefore, the major conclusion is that adsorption on clays can largely determine the diurnal water vapor cycle (Jakosky et al., 1997), but that this effect will only be important in the tropical to equatorial regions.

However the previous conclusion is based only on the thermodynamics of the adsorption process (i.e. isotherms, and equilibrium conditions). An important result is that the kinetics of water adsorption is also strongly dependent on the temperature (see Section 4.3 and Fig. 11). Studies by Zent et al. (2001) showed that the kinetics of water uptake are slower at 211 K compared to 273 K by about a factor of ten. Therefore, if clays can account for the diurnal variability from an equilibrium point of view, their rate of adsorption at low temperature may prevent them from being an efficient adsorbent on Mars. However, our kinetic constants are all determined between 270 and 275 K, which prevent any kinetic calculations for martian temperatures. However, if the active layer is 100 times thinner than the limit thickness, the timescale should be extremely short (Fig. 5).

5. Conclusions

We have performed an extensive study of the interaction of water vapor with a clay regolith during the sublimation of shallow ice under simulated martian conditions (7 mbar, 265–273 K). We determined the corresponding diffusion coefficient ($1.29 \pm 0.06 \times 10^{-4}$ $\text{m}^2\,\text{s}^{-1}$) as well as the adsorption constants using both Langmuir and BET theories (respectively $4.9 \pm 1.0 \times 10^{-2}$ Pa^{-1} and 30 ± 10). Our results show that both diffusion and adsorption are important in understanding regolith–water interactions (Jakosky, 1983; Zent et al., 1993), sometimes acting simultaneously. At shallow depths of overlying clay (<10 mm) the sublimation rate is controlled by adsorption and both diffusion through the atmosphere and the clay layer. Deeper layers show control by adsorption and diffusion through the regolith only. Once the regolith is has reached its maximum adsorption capacity, the diffusion process alone controls the transport of water vapor.

Our diffusion coefficients suggest that diffusion through silt size montmorillonite clay is not a barrier to ice sublimation at long timescales, in accordance with previous theoretical studies (Schorghofer and Aharonson, 2005). Temperature remains the main parameter controlling the sublimation rate. However, at low subsurface martian temperatures, ice deposited in previous glaciations periods, especially at mid to high latitudes, could still be present and thus account for the detection of shallow water by the GRS on Mars Odyssey.

Moreover, clays have important adsorption properties that make them a potential reservoir of subsurface water. Because the amount of adsorbed water in clays is large a very thin layer can control the diurnal cycle, provided that the average temperature remains in the range 210 to 270 K and the amplitude of humidity variation is not too extreme. The clay layer required to adsorb water remains generally inferior to the thermal skin depth allowing clays to thermodynamically control the diurnal cycle.

Acknowledgments

We are grateful to Walter Graupner for laboratory assistance, as well as Larry Roe and Rick Ulrich for discussions. We also thank Pr. Stephen Clifford and the anonymous reviewer for their comments that helped improving the quality of this manuscript. A major award from the W.M. Keck Foundation, Los Angeles, CA, supports the laboratory and present work.

References

Anderson, D.M., Gaffney, E.S., Low, P.F., 1967. Frost phenomena on Mars. Science 155 (3760), 319–322.

Anderson, D.M., Schwarz, M.J., Tice, A.R., 1978. Water vapor adsorption by sodium montmorillonite at −5 °C. Icarus 34, 638–644.

Bandfield, J.L., 2007. High-resolution subsurface water-ice distributions on Mars. Nature 447, 64–67.

Bibring, J.P., Langevin, Y., Poulet, F., Gendrin, A., Gondet, B., Berthé, M., Soufflot, A., Drossart, P., Combes, M., Bellucci, G., Moroz, V., Mangold, N., Schmitt, B., Omega team, 2004. Perennial water ice identified in the south polar caps of Mars. Nature 428, 627–630.

Boynton, W.V., Feldman, W.C., Squyres, S.W., Prettyman, T.H., Brückner, J., Evans, L.G., Reedy, R.C., Starr, R., Arnold, J.R., Drake, D.M., Englert, P.A.J., Metzger, A.E., Mitrofanov, I., Trombka, J.I., d'Uston, C., Wänke , H., Gasnault, O., Hamara, D.K., Janes, D.M., Marcialis, R.L., Maurice, S., Mikheeva, I., Taylor, G.J., Tokar, R., Shinohara, C., 2002. Distribution of hydrogen in the near surface of Mars: Evidence for subsurface ice deposits. Science 297, 81–85.

Brunauer, S., Emmett, P.H., Teller, E., 1938. Adsorption of gases in multimolecular layers. J. Am. Chem. Soc. 60, 309–319.

Bryson, K., Chevrier, V., Sears, D.W.G., 2008. Ice on Mars: An experimental investigation into the increased stability of ice on Mars by a surface covering of fine-grained basaltic regolith. Icarus 196, 459–476.

Chevrier, V., Sears, D.W.G., Chittenden, J., Roe, L.A., Ulrich, R., Bryson, K., Billingsley, L., Hanley, J., 2007. The sublimation rate of ice under simulated Mars conditions and the effect of layers of mock regolith JSC Mars-1. Geophys. Res. Lett. 34, doi:10.1029/2006GL028401. L02203.

Clifford, S.M., Hillel, D., 1983. The stability of ground ice in the equatorial region of Mars. J. Geophys. Res. 88, 2456–2474.

Cooper, C.D., Mustard, J.F., 2002. Spectroscopy of loose and cemented sulfate-bearing soils: Implications for duricrust on Mars. Icarus 158, 42–55.

Fanale, F.P., Cannon, W.A., 1971. Adsorption on the martian regolith. Nature 230, 502–504.

Farmer, C.B., 1976. Liquid water on Mars. Icarus 28, 279–289.

Farmer, C.B., Doms, P.E., 1979. Global seasonal variations of water vapor on Mars and the implications for permafrost. J. Geophys. Res. 84, 2881–2888.

Feldman, W.C., Mellon, M.T., Maurice, S., Prettyman, T.H., Carey, J.W., Vaniman, D.T., Bish, D.L., Fialips, C.I., Chipera, S.J., Kargel, J.S., Elphic, R.C., Funsten, H.O., Lawrence, D.J., Tokar, R.L., 2004a. Hydrated states of $MgSO_4$ at equatorial latitudes on Mars. Geophys. Res. Lett. 31, doi:10.1029/2004GL020181. L16702.

Feldman, W.C., Prettyman, T.H., Maurice, S., Plaut, J.J., Bish, D.L., Vaniman, D.T., Mellon, M.T., Metzger, A.E., Squyres, S.W., Karunatillake, S., Boynton, W.V., Elphic, R.C., Funsten, H.O., Lawrence, D.J., Tokar, R.L., 2004b. Global distribution of near-surface hydrogen on Mars. J. Geophys. Res. 109, doi:10.1029/2003JE002160. E09006.

Flasar, F.M., Goody, R.M., 1976. Diurnal behavior of water on Mars. Planet. Space Sci. 24, 161–181.

Hart, H.M., Jakosky, B.M., 1986. Composition and stability of the condensate observed at the Viking Lander 2 site on Mars. Icarus 66, 134–142.

Head III, J.W., Kreslavsky, M.A., Pratt, S., 2002. Northern lowlands of Mars: Evidence for widespread volcanic flooding and tectonic deformation in the Hesperian Period. J. Geophys. Res. 107 (E1), doi:10.1029/2000JE001445. 5004.

Head, J.W., Mustard, J.F., Kreslavsky, M.A., Milliken, R.E., Marchant, D.R., 2003. Recent ice ages on Mars. Nature 426, 797–802.

Head, J.W., Marchant, D.R., Agnew, M.C., Fassett, C.I., Kreslavsky, M.A., 2006a. Extensive valley glacier deposits in the northern mid-latitudes of Mars: Evidence for Late Amazonian obliquity-driven climate change. Earth Planet. Sci. Lett. 241, 663–671.

Head, J.W., Nahm, A.L., Marchant, D.R., Neukum, G., 2006b. Modification of the dichotomy boundary on Mars by Amazonian mid-latitude regional glaciation. Geophys. Res. Lett. 33, doi:10.1029/2005GL024360. L08S03.

Hess, S.T., Henry, R.M., Leovy, C.B., Ryan, J.A., Tillman, J.E., 1977. Meteorological results from the surface of Mars: Viking 1 and 2. J. Geophys. Res. 82, 4559–4574.

Houben, H., Haberle, R.M., Young, R.E., Zent, A.P., 1997. Modeling the martian seasonal water cycle. J. Geophys. Res. 102 (E4), 9069–9083.

Hudson, T.L., Aharonson, O., Schorghofer, N., Farmer, C.B., Hecht, M.H., Bridges, N.T., 2007. Water vapor diffusion in Mars subsurface environments. J. Geophys. Res. 112 (E5), doi:10.1029/2006JE002815. E05016.

Ingersoll, A.P., 1970. Mars: Occurrence of liquid water. Science 168 (3934), 972–973.

Jakosky, B.M., 1983. The role of seasonal reservoirs in the Mars water cycle. I. Seasonal exchange of water with the regolith. Icarus 55, 1–18.

Jakosky, B.M., 1985. The seasonal cycle of water on Mars. Space Sci. Rev. 41 (1–2), 131–200.

Jakosky, B.M., Christensen, P.R., 1986. Global duricrust on Mars—Analysis of remote-sensing data. J. Geophys. Res. 91, 3547–3559.

Jakosky, B.M., Zent, A.P., Zurek, R.W., 1997. The Mars water cycle: Determining the role of exchange with the regolith. Icarus 130, 87–95.

Jakosky, B.M., Mellon, M.T., Varnes, E.S., Feldman, W.C., Boynton, W.V., Haberle, R.M., 2005. Mars low-latitude neutron distribution: Possible remnant near-surface water ice and a mechanism for its recent emplacement. Icarus 175, 58–67.

Leighton, R.B., Murray, B.C., 1966. Behavior of carbon dioxide and other volatiles on Mars. Science 153, 136–144.

Mellon, M.T., Jakosky, B.M., 1993. Geographic variations in the thermal and diffusive stability of ground ice on Mars. J. Geophys. Res. 98, 3345–3364.

Mellon, M.T., Phillips, R.J., 2001. Recent gullies on Mars and the source of liquid water. J. Geophys. Res. 106 (E10), 23165–23180.

Mellon, M.T., Feldman, W.C., Prettyman, T.H., 2004. The presence and stability of ground ice in the southern hemisphere of Mars. Icarus 169, 324–340.

Milkovich, S.M., Head, J.W., Marchant, D.R., 2006. Debris-covered piedmont glaciers along the northwest flank of the Olympus Mons scarp: Evidence for low-latitude ice accumulation during the Late Amazonian of Mars. Icarus 181, 388–407.

Mooney, R.W., Keenan, A.G., Wood, L.A., 1952. Adsorption of water vapor by montmorillonite. I. Heat of desorption and application of BET theory. J. Am. Chem. Soc. 74 (6), 1367–1371.

Moore, S.R., Sears, D.W.G., 2006. On laboratory simulation and the effect of small temperature oscillations about the freezing point and ice formation on the evaporation rate of water on Mars. Astrobiology 6 (4), 644–650.

Neukum, G., Jaumann, R., Hoffmann, H., Hauber, E., Head, J.W., Basilevsky, A.T., Ivanov, B.A., Werner, S.C., van Gasselt, S., Murray, J.B., McCord, T., T.H.C.-I. team, 2004. Recent and episodic volcanic and glacial activity on Mars revealed by the High Resolution Stereo Camera. Nature 432, 971–979.

Paige, D.A., 1992. The thermal stability of near-surface ground ice on Mars. Nature 356, 43–45.

Poulet, F., Bibring, J.-P., Mustard, J.F., Gendrin, A., Mangold, N., Langevin, Y., Arvidson, R.E., Gondet, B., Gomez, C., OMEGA team, 2005. Phyllosilicates on Mars and Implications for the Early Mars History. Nature 481, 623–627.

Schofield, J.T., Barnes, J.R., Crisp, D., Haberle, R.M., Larsen, S., Magalhaes, J.A., Murphy, J.R., Seiff, A., Wilson, G., 1997. The Mars Pathfinder Atmospheric Structure Investigation/Meteorology (ASI/MET) Experiment. Science 278, 1752–1757.

Schorghofer, N., 2007. Dynamics of ice ages on Mars. Nature 449, 192–195.

Schorghofer, N., Aharonson, O., 2005. Stability and exchange of subsurface ice on Mars. J. Geophys. Res. 110, doi:10.1029/2004JE002350. E05003.

Sears, D.W.G., Chittenden, J.D., 2005. On laboratory simulation and the temperature dependence of evaporation rate of brine on Mars. Geophys. Res. Lett. 32, doi:10.1029/2005GL024154. L23203.

Sears, D.W.G., Moore, S.R., 2005. On laboratory simulation and the evaporation rate of water on Mars. Geophys. Res. Lett. 32, doi:10.1029/2005GL023443. L16202.

Smith, M.D., 2002. The annual cycle of water vapor on Mars as observed by the Thermal Emission Spectrometer. J. Geophys. Res. 107 (E11), doi:10.1029/2001JE001522. 5115.

Smith, P.H., Bell III, J.F., Bridges, N.T., Britt, D.T., Gaddis, L., Greeley, R., Keller, H.U., Herkenhoff, K.E., Jaumann, R., Johnson, J.R., Kirk, R.L., Lemmon, M., Maki, J.N., Malin, M.C., Murchie, S.L., Oberst, J., Parker, T.J., Reid, R.J., Sablotny, R., Soderblom, L.A., Stoker, C., Sullivan, R., Thomas, N., Tomasko, M.G., Ward, W., Wegryn, E., 1997. Results from the Mars Pathfinder Camera. Science 278, 1758–1764.

Smoluchowski, R., 1968. Mars: Retention of ice. Science 159 (3821), 1348–1350.

Sprague, A.L., Hunten, D.M., Doose, L.R., Hill, R.E., 2003. Mars atmospheric water vapor abundance: 1996–1997. Icarus 163, 88–101.

Sprague, A.L., Hunten, D.M., Doose, L.R., Hill, R.E., Boynton, W.V., Smith, M.D., Pearl, J.C., 2006. Mars atmospheric water vapor abundance: 1991–1999, emphasis 1998–1999. Icarus 184, 372–400.

Wall, S.D., 1981. Analysis of condensates formed at the Viking 2 lander site—The first winter. Icarus 47, 173–183.

Zent, A.P., Haberle, R.M., Houben, H.C., Jakosky, B.M., 1993. A coupled subsurface-boundary layer model of water on Mars. J. Geophys. Res. 98 (E2), 3319–3337.

Zent, A.P., Howard, D.J., Quinn, R.C., 2001. H_2O adsorption on smectites: Application to the diurnal variation of H_2O in the martian atmosphere. J. Geophys. Res. 106 (7), 14667–14674.

Zent, A.P., Quinn, R.C., 1995. Simultaneous adsorption of CO_2 and H_2O under Mars-like conditions and application to the evolution of the martian climate. J. Geophys. Res. 100 (E3), 5341–5349.

Zent, A.P., Quinn, R.C., 1997. Measurement of H_2O under Mars-like conditions: Effects of adsorbent heterogeneity. J. Geophys. Res. 102 (E4), 9085–9095.